Development of Single-Site Heterogeneous Catalysts Constructed within Porous Materials and Their Highly Selective Catalytic Reactivities

Development of Single-Site Heterogeneous Catalysts Constructed within Porous Materials and Their Highly Selective Catalytic Reactivities

（多孔性材料内に構築した不均一系シングルサイト触媒の開発とそれらの高選択的な触媒反応性）

Masakazu Saito

齋藤 雅和

February 2013

Doctoral Thesis at Osaka Prefecture University

Contents

Chapter 1

General Introduction

Backgrounds

In recent years, the environmental issues have attracted much interest at a global scale since the destruction of our environment by the exhaust of toxic agents as well as the consumption of natural resources have been accelerated by global population growth. In this regard, sustainable green chemistry, which focuses on the development and usages of environmentally friendly and safe processes, is considered to be an important concept in the field of science [1]. In line with such work, catalysts have been focus of much attention as key materials to achieve such a sustainable production of new safe and clean chemical compounds and processes.

The catalysts can be divided into two main types, which are heterogeneous and homogeneous catalysts. In a homogeneous reaction, the catalyst is in the same phase as the reactants, while in a heterogeneous reaction, the catalyst is in a different phase from the reactants. The homogeneous catalysts frequently exhibit very high activity and selectivity compared with heterogeneous catalysts; however, their use on a large scale is often complicated by difficulties associated with their separation from the reaction products and also with of corrosion [2]. Considering the application for the industrial process, the catalyst is desired to be separated and recovered from reaction products as well as recycled for the next reaction cycles. Since heterogeneous catalysts satisfy above requirements due to their insoluble properties, the change from homogeneous into heterogeneous catalysts is strongly desired for the development of green-chemical processes. Among various heterogeneous catalysts, the single-site heterogeneous catalysts, which possess uniform catalytic active sites, are one of the most promising candidates for the design of efficient and clean catalytic systems as well as the development of more highly active and selective catalytic reactions [3].

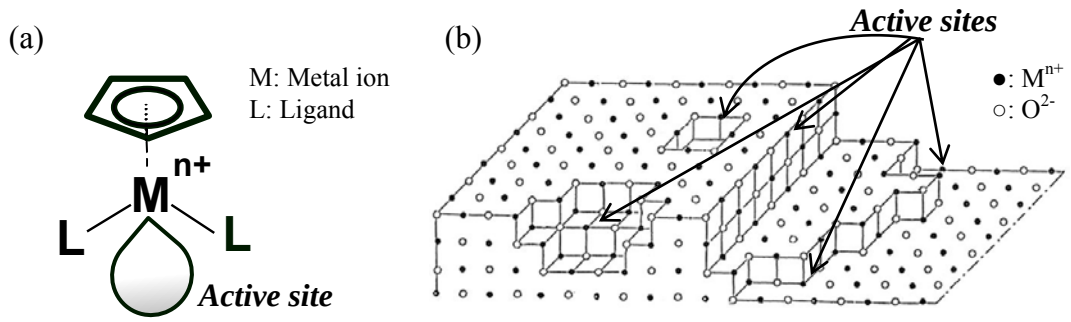

Figure 1.1 Active sites of (a) organometallic complex (homogeneous catalyst) and (b) bulk metal oxide (heterogeneous catalyst).

Single-Site Catalysts

In homogeneous catalysts, such as organometallic complexes, catalytically active single-sites are easily designed by controlling the coordination ligands (Figure 1.1(a)) [4-7]. The single-site catalysts having uniform catalytic active sites promote the various organic reactions with high selectivity because reactions proceed through a certain catalytic reaction process on them. On the other hand, heterogeneous catalysts including solid catalysts exhibit relatively low selectivity because active sites on their catalytic surfaces are not uniform (Figure 1.1 (b)) [8-9]. However, the strictly regulated active-sites on solid surfaces formed by using various physical and chemical methods are applicable to single-site catalysts. For example, highly dispersed metal oxide species immobilized on various supports are well known to act as single-site catalysts or photocatalysts [10-25]. In our previous works, an organoruthenium complex was successfully constructed within phenylene–bridged inorganic-organic hybrid mesoporous materials (HMM–ph) by a simple ligand exchange reaction [26-29]. In this complex, the metal center is directly coordinated with phenylene moiety of HMM–ph that behave as a “framework ligand”. The present study deals with the development of highly active and selective single-site heterogeneous catalysts and photocatalysts.

Microporous and Mesoporous Materials

Zeolites are aluminosilicate microporous materials and known as one of the "molecular sieves". The term “molecular sieve” refers to a particular property of these materials, i.e., the ability to selectively sort molecules based on a size exclusion process. This unique ability is due to a very regular pore structure of molecular dimensions. The maximum size of the molecular or ionic species that can enter the pores of a zeolite is controlled by the dimensions of the channels [30]. Zeolites are widely used in industry for water purification as catalysts, the preparation of advanced materials and nuclear reprocessing [31].

On the other hand, mesoporous materials are a class of 2D– and 3D–nanostructured materials with well-defined mesoscale pores (2–50 nm diameter) and surface areas reaching 1000 m^2/g [32]. Mesoporous materials are formed by a self-assembly process from mixed solutions of sol-gel precursors (e.g. metal alkoxides) and structure-directing amphiphiles such as block-copolymers or surfactants [33,34]. These mesoporous materials are expected to be used as catalysts, adsorbents, gas sensing materials, ion exchange and optical materials [18-20,35-37]. The researches in the field of porous materials have steadily grown.

Recently, novel inorganic-organic hybrid mesoporous materials (HMMs), well known as periodic mesoporous organosilicas, having uniformly distributed organic bridging groups as integral components of the framework have been developed [38]. HMMs, prepared via the condensation of bis(trialkoxysilyl)organics $(R'O)_3Si–R–Si(OR')_3$ (R = $–C_2H_4–$, $–C_6H_4–$, $–(C_6H_4)_2–$, etc.), have attracted attention in the fields of adsorbents, sensors and light harvesting or emitting optical devices [51].

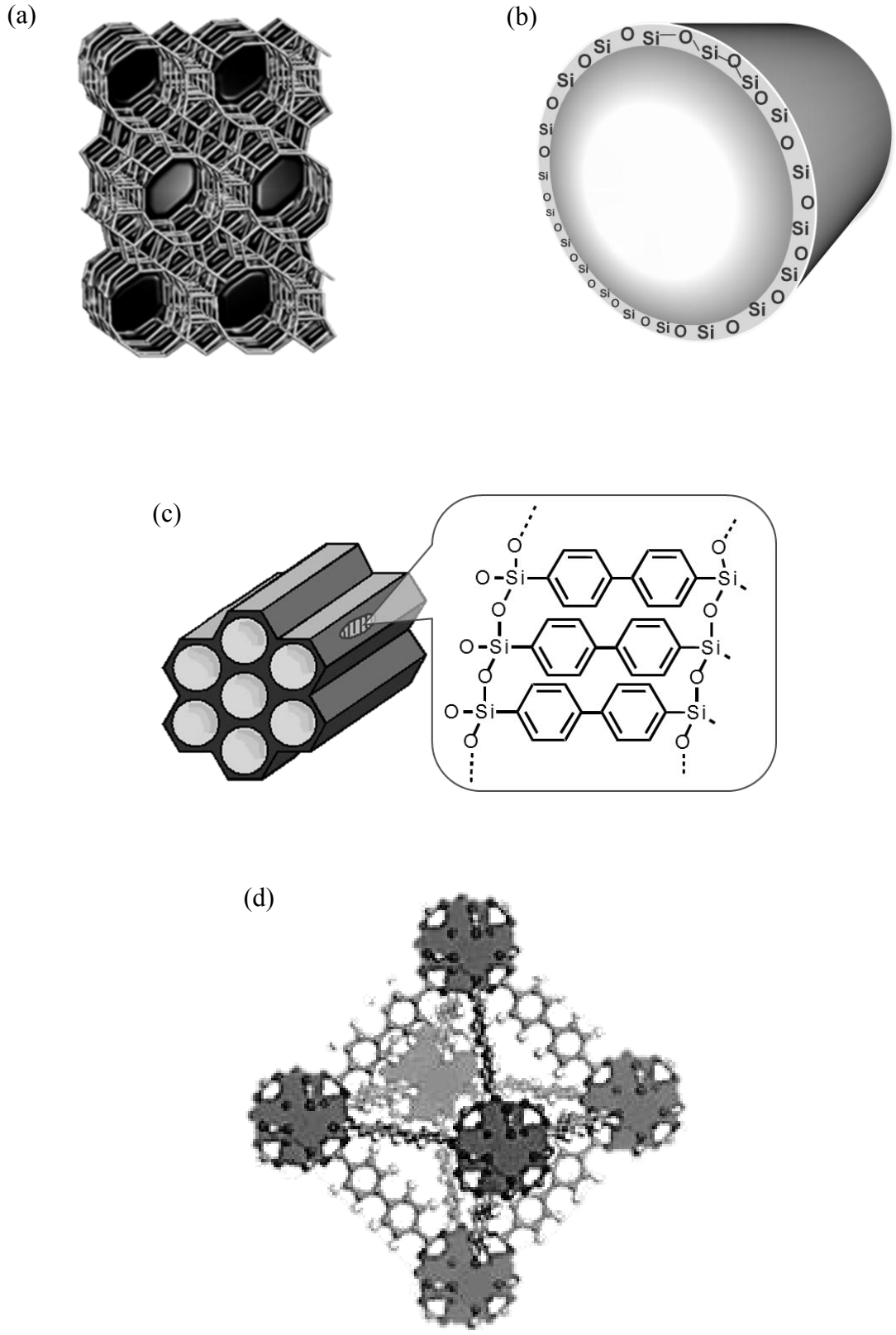

Figure 1.2 Porous structures of (a) BEA zeolite, (b) MCM-41, (c) HMM-biph and (d) Zr-based MOFs.

Besides HMMs, metal–organic frameworks (MOFs) having 3–dimensional network structures constructed from organic linkers and metal-oxo clusters have attracted attention in the fields of catalysts, adsorbents and separation materials owing to their extremely large surface areas and pore volumes and structural diversity that enables rational material design [52-56]. The functionalization of MOFs by introducing substituent groups, such as $–NH_2$ and $–SO_3H$ groups, into their organic linkers is promising techniques to control their chemical properties and to form catalytically active sites for organic synthesis [57,58]. In this thesis, these microporous and mesoporous materials were applied for the support of single-site catalysts.

Outline of Thesis

This study was performed to develop preparation methods for the incorporation of single-site catalysts within the frameworks of microporous and mesoporous materials. The active site structures and their reaction fields of objective single-site catalysts were controlled at atomic or molecule level in microporous and mesoporous materials by using post-synthesis, ligand exchange reaction and chemical vapor deposition (CVD) methods. Local structures of active sites and porous structures of catalytic supports were characterized by UV–Vis, photoluminescence, FT–IR, TPD, XAFS, XRD and N_2 adsorption isotherms measurements. The synthesized single-site catalysts were applied for various selective heterogeneous reactions.

This thesis contains 7 chapters, the first being an overall introduction of the research objectives with outlines of the succeeding chapters summarized as follows:

Chapter 2 deals with photocatalytic activities of highly dispersed isolated Ti^{4+} ion species within the framework of BEA zeolite prepared by a two-step post-synthesis method (TiSiBEA). In this chapter, the characterizations of the local structure and photo-excited

state of the active site in TiSiBEA as well as the photocatalytic activities for the oxidation of CO with N_2O and decomposition of 2-propanol in water are discussed.

Chapter 3 deal with the preparation, characterization and catalytic properties of tin triflate species incorporated within mesoporous silicas. In the homogeneous systems, the metal triflates fall into an interesting category of catalysts having high water tolerance [59]. Here, the highly dispersed tin species in mesoporous silicas are treated with triflic acid to form tin triflate within their silica frameworks (SnOTf-MCM-41). The characterizations of the local structure and acid property of the active site are performed by various spectroscopies. Moreover, the catalytic activity of SnOTf-MCM-41 for Mukaiyama aldol reactions of benzaldehyde with 1-trimethylsiloxy cyclohexene is examined at room temperature.

Chapter 4 focuses on the formation of organoruthenium complexes in the biphenylene-bridged and phenylene-bridged inorganic organic hybrid materials (HMM–biph and HMM–ph) through a ligand exchange reaction. In homogeneous system, the $C_6H_6RuCpPF_6$ (Cp: cyclopentadienyl) complex is known to show an unique photochemical behavior in which it easily converts to $(CH_3CN)_3RuCpPF_6$ complex in acetonitrile under UV irradiation, while the three acetonitrile ligands of $(CH_3CN)_3RuCpPF_6$ complex is reversely converted to benzene ligand by heat treatment in benzene [60]. Using this behavior, the organoruthenium complexes are formed in the inorganic organic hybrid materials by coordination with phenylene and biphenylene moieties as framework ligands. Moreover, the thus-formed complexes within HMMs are applied for the selective hydrosilylation reaction of 1-hexyne with triethylsilane as heterogeneous catalysts.

Chapter 5 gives the detail of the enhanced catalytic activity of arenetricarbonyl chromium complexes constructed within Zr-Based MOFs by introducing substituents into organic linkers of the MOFs. The functionalization of MOFs by introducing substituent groups into their organic linkers as well as the formation of organometallic complexes with their organic

linkers are promising techniques to control their chemical properties and to form catalytically active sites for organic synthesis. In this chapter, catalytic activities of formed arenetricarbonyl chromium complexes in Zr-based MOFs having substituent groups for heterogeneous dehydrochlorination of 2-chloro-2-methylbutane are discussed.

Chapter 6 discusses the effect of pore size on catalytic activities of arenetricarbonyl complexes ([–$C_6H_4M(CO)_3$–]; M = Mo, Cr) constructed within Zr-Based MOFs. The influences of kinds of metal center as well as pore size on catalytic activities of [–$C_6H_4M(CO)_3$–] complexes constructed within Zr-Based MOFs for epoxidation of cyclooctene with tertiary butylhydroperoxide (TBHP) are investigated.

In the final Chapter 7, the results and conclusions of the various investigations covered in this thesis have been summarized.

References

[1] P.T. Anastas, J.B. Zimmerman, Environ. Sci. Technol., **37**, 94A (2003).

[2] M.S. Scnrrell, Platinum Metals Rev., **21**, 92 (1977).

[3] J.M. Thomas, R. Raja, D.W. Lewis, Angew. Chem. Int. Ed., **44**, 6456 (2005).

[4] J.J. Concepcion, M-K. Tsai, J.T. Muckerman, T.J. Meyer, J. Am. Chem. Soc., **132**, 1545 (2010).

[5] M.H. Chisholm, Inorganica Chimica Acta, **362**, 4284 (2009).

[6] S. Mark, A. Kurek, R. Mülhaupt, R. Xu, G. Klatt, H. Köppel, M. Enders, Angew. Chem. Int. Ed., **49**, 8751 (2010).

[7] W-M. Ren, Z-W. Liu, Y-Q. Wen, R. Zhang, X-B. Lu, J. Am. Chem. Soc., **131**, 11509 (2009).

[8] B.M. Bhanage, S. Fujita, Y. Ikushima, M. Arai, Appl. Catal. A: General, **219**, 259 (2001).

[9] T. Blasco, J.M. Nieto, Appl. Catal. A: General, **157**, 117 (1997).

[10] N.K. Mal, A.V. Ramaswamy, J. Mol. Catal. A Chem., **105**, 149 (1996).

[11] R. Garro, M.T. Navarro, J. Primo, A. Corma, J. Catal., **233**, 342 (2005).

[12] S.M. Coman, G. Pop, C. Stere, V.I. Parvulescu, J.E. Haskouri, D. Beltran, P. Amoros, J. Catal., **251**, 388 (2007).

[13] N. Candu, S.M. Coman, V.I. Parvulescu, J.E. Haskouri, P. Amoros, D. Beltran, Top. Catal., **52**, 571 (2009).

[14] V.I. Parvulescu, S.M. Coman, N. Candu, J.E. Haskouri, D. Beltran, P. Amoros, J. Mater. Sci., **44**, 6693 (2009).

[15] M. Verziu, J.E. Haskouri, D. Beltran, P. Amoros, D. Macovei, N.G. Gheorghe, C.M. Teodorescu, S.M. Coman, V.I. Parvulescu, Top. Catal., **53**, 763 (2010).

[16] T.R. Gaydhankar, P.N. Joshi, P. Kalita, R. Kumar, J. Mol. Catal. A Chem., **265**, 306 (2007).

[17] K. Chaudhari, T.K. Das, P.R. Rajmohanan, K. Lazar, S. Sivasanker, A. Chandwadkar, J. Catal., **183**, 281 (1999).

[18] M. Sasidharan, S.V.N. Raju, K.V. Srinivasan, V. Paul, R. Kumar, Chem. Commun., 129 (1996).

[19] M. Sasidharan, R. Kumar,, J.Catal., **220**, 326 (2003).

[20] M. Kitano, K. Nakajima, J.N. Kondo, S. Hayashi, M. Hara, J. Am. Chem. Soc., **132**, 6622 (2010).

[21] E. A. Quadrelli, J-M. Basset, Coord. Chem. Rev., **254**, 707 (2010).

[22] M. Anpo, T-H. Kim, M. Matsuoka, Catal. Today, **142**, 114 (2009).

[23] T. Kamegawa, T.-H. Kim, J. Morishima, M. Matsuoka, M. Anpo, Catal. Lett., **129**, 7 (2008).

[24] T. Kamegawa, M. Matsuoka, M. Anpo, Res. Chem. Intermed., **34**, 427 (2007).

[25] M. Anpo, J.M. Thomas, Chem. Commun., 3273 (2006).

[26] A.C. Coelho, S.S. Balula, S.M. Bruno, J.C. Alonso, N. Bion, P. Ferreira, M. Pillinger, A.A. Valente, J. Rocha, I.S. Gonc¸alves, Adv. Synth. Catal., **352** 1759 (2010).

[27] A. C. Coelho, S. S. Balula, M. M. Antunes, T. I. Gerganova, N. Bion, P. Ferreira, M. Pillinger, A. A. Valente, J. Rocha, I. S. Goncalves, J. Mol. Catal. A: Chem., **332**, 13 (2012).

[28] T. Kamegawa, M. Saito, T. Watanabe, K. Uchihara, M. Kondo, M. Matsuoka, M. Anpo, J. Mater. Chem., **21**, 12228 (2011).

[29] T. Kamegawa, M. Saito, T. Sakai, M. Matsuoka, M. Anpo, Catal. Today, **181**, 14 (2012).

[30] M. Moliner, J. Gonzalez, M.T. Portilla, T. Willhammar, F. Rey, F.J. Llopis, X. Zou, A. Corma, J. Am. Chem. Soc., **133**, 9497 (2011).

[31] VK Saini, J Pires, J. Chem. Educ., **89**, 276 (2012).

[32] J. Beck, J.C. Vartuli, Curr. Opin. Solid State Mater. Sci., **1**, 76 (1996).

[33] J.S. Beck, J.C. Vartuli, W.J. Roth, M. E. Leonowicz, C. T. Kresge, K. D. Schmitt, C. T. W. Chu, D. H. Olson, E. W. Sheppard, S. B. McCullen, J. B. Higgins, J. L. Schlenker, J. Am. Chem. Soc.,**114**, 10834 (1992).

[34] Y. Wan, D. Zhao, Chem. Rev., **107**, 2821 (2007).

[35] K. Moller, T. Bein, Chem. Mater., **10**, 2950 (1998).

[36] Y. D. Wang, C. L. Ma, X. H. Wu, X.D. Sun, H.D. Li, Sens. Act. B: Chem., **85**, 270 (2002).

[37] G, Schulz-Ekloff, D. Wöhrle, B. van Duffel, R.A. Schoonheydt, Micropor. Mesopor. Mater., **51**, 91 (2002).

[38] T. Asefa, M. Kruk, M.J. MacLachlan, N. Coombs, H. Grondey, M. Jaroniec, G.A. Ozin, J. Am. Chem. Soc., **123**, 8520 (2001).

[39] S. Inagaki, S. Guan, Y. Fukushima, T. Ohsuna, O. Terasaki, J. Am. Chem. Soc., **121**,

9611 (1999).

[40] B.J. Melde, B.T. Holland, C.F. Blanford, A. Stein, Chem. Mater., **11**, 3302 (1999).

[41] T. Asefa, M.J. MacLachlan, N. Coombs, G.A. Ozin, Nature, **402**, 867 (1999).

[42] C. Yoshina-Ishii, T. Asefa, N. Coombs, M.J. MacLachlan, G.A. Ozin, Chem. Commun., 2539 (1999).

[43] F. Hoffmann, M. Cornelius, J. Morell, M. Fröba, Angew. Chem., Int. Ed., **45**, 3216 (2006).

[44] S. Fujita, S. Inagaki, Chem. Mater., **20**, 891 (2008).

[45] A. Stein, B.J. Melde, R.C. Schroden, Adv. Mater., **12**, 1403 (2000).

[46] A. Sayari, S. Hamoudi, Y. Yang, I.L. Moudrakovsk, J.R. Ripmeester, Chem. Mater., **12**, 3857 (2000).

[47] M. P. Kapoor, Q. Yang, S. Inagaki, J. Am. Chem. Soc., **124**, 15176 (2002).

[48] M. Cornelius, F. Hoffmann, M. Fröba, Chem. Mater., **17**, 6674 (2005).

[49] S. Inagaki, S. Guan, T. Ohsuna, O. Terasaki, Nature, **416**, 304 (2002).

[50] T. Tani, N. Mizoshita, S. Inagaki, J. Mater. Chem., **19**, 4451 (2009).

[51] S. Inagaki, O. Ohtani, Y. Goto, K. Okamoto, M. Ikai, K. Yamanaka, T. Tani, T. Okada, Angew. Chem., Int. Ed., **48**, 4042 (2009).

[52] K. Schlichte, T. Kratzke, S. Kaskel, Micropor. Mesopor. Mater., **73**, 81 (2004).

[53] R. Banerjee, A. Phan, B. Wang, C. Knobler, H. Furukawa, M. O_Keeffe, O. M. Yaghi, Science, **319**, 939 (2008).

[54] S. Kitagawa, R. Kitaura, S. Noro, Angew. Chem., Int. Ed., **43**, 2334 (2004).

[55] M. Dinca, J. R. Long, J. Am. Chem. Soc., **127**, 9376 (2005).

[56] H. Bux, F. Liang, Y. Li, J. Cravillon, M. Wiebcke, J. Caro, J. Am. Chem. Soc., **131**, 16000 (2009).

[57] F. Vermoortele, R. Ameloot, A. Vimont, C. Serrec, D.D. Vos, Chem. Commun., **47**, 1521

(2011).

[58] G. Akiyama, R. Matsuda, H. Sato, M. Takata, S. Kitagawa, Adv. Mater., **23**, 3294 (2011).

[59] E. Altman, G.D. Stefanidis, T.V. Gerven, A. Stankiewicz, Ind. Eng. Chem. Res., **51**, 1612 (2012).

[60] T.P. Gill, K.R. Mann, Organometallics, **1**, 485 (1982).

Chapter 2

Influence of The Ti Content on The Photocatalytic Oxidation of 2-propanol and CO on TiSiBEA Zeolites

2.1. Introduction

Transition metal ions well dispersed in zeolite frameworks are considered to be the active sites of photocatalytic processes [1]. We have shown that the incorporation of vanadium ions into the framework T–atom sites of BEA zeolite is strongly favoured when, in a first step, BEA is dealuminated by treatment with a nitric acid solution leading to the so called SiBEA zeolite which upon contact with an aqueous NH_4VO_3 solution in a second step reacts with cationic monomer V species via the SiO–H groups of vacant T–atom sites created in the first step [2-4].

Using the latter method and transition metal complexes in aqueous solutions, tetrahedral Co(II), Fe(III) or Cu(II) ions have been incorporated into the BEA framework [5-7].

Recently, the two-step postsynthesismethod has been extended to gas phase precursors such as $TiCl_4$ vapor with the advantage to restrict the speciation of titanium to one single type of species as shown earlier by the grafting of $VOCl_3$ onto silica [8,9]. Thus isolated tetrahedral Ti^{4+} ions were successfully incorporated into the BEA framework. Such tetrahedral Ti^{4+} species are known to be active in photocatalytic processes such as the decomposition of NO into N_2 and O_2, the reduction of CO_2 with H_2O, the oxidation of CO or the epoxidation of olefins [1,10-12]. The incorporation of Ti into the SiBEA framework was evidenced by XRD, ^{29}Si-MAS NMR, ^{1}H–^{29}Si-CP MAS NMR and ^{1}H-MAS NMR [8,13]. DR UV–Vis and XPS investigations show that mainly framework tetrahedral Ti^{4+} ions are present in Ti_xSiBEA zeolites.

The aim of the present work is to investigate the effect of Ti content on the activity of TiSiBEA zeolites in the: photocatalytic liquid phase oxidation of 2-propanol and gas phase oxidation of CO.

2.2. Experimental

Catalyst preparation

To control the formation of tetrahedral Ti^{4+} species in the framework of BEA zeolite, we have used two-step postsynthesis method reported earlier for incorporation of V which have been modified to incorporate Ti and consist, in the first step, the creation of vacant T–atom sites in zeolite structure by dealumination of tetraethylammonium BEA, provided by RIPP (China),with a 13 mol/L HNO_3 solution (4 h, 353 K) and then, in the second step, incorporation of Ti into resulting SiBEA zeolite (Si/Al > 1300) by reacting $TiCl_4$ vapor with the silanol groups of vacant T–atom sites [2].

In order to incorporate Ti ions in vacant T-atom sites, 2 g of SiBEA were treated in a fixed-bed reactor at 423 K for 3 days in flowing oxygen. The solid was subjected at 573 K for 2, 6 and 16 h, to a nitrogen flow (100 mL/min) through a saturator containing liquid $TiCl_4$ (Aldrich, purity 99.9%) at 266 K, as described earlier for the preparation of mesoporous TiMCM-41 [14]. The $TiCl_4$ vapor pressure in the saturator was 200 Pa and the volume to volume (v/v) ratio of $TiCl_4/N_2$ was 0.2%. The resulting solids were cooled to room temperature, exposed to moist air for 12 h, dried in air at 353 K for 12 h and finally calcined in flowing dry air at 723 K for 4 h. The solids obtained will be hereafter referred to Ti_xSiBEA (x=1.5, 3.2 and 5.8 Ti wt.%).

Catalyst characterization

Chemical analysis of titanium was performed by inductively coupled plasma spectrometry at the Service Central d'Analyse, CNRS, Vernaison, France. Powder X-ray diffractograms were recorded on a Siemens D5000 apparatus using the CuKα radiation (λ = 154.05 pm). DR UV–Vis spectra were recorded on a Cary 5E spectrometer equipped with a double integrator using $BaSO_4$ as reference. Photoluminescence spectra were recorded at 77 K with

a Spex Fluorolog II Jobin-Yvon spectrofluorimeter (equipped with 460W Xe lamp as excitation source, and color filters to eliminate scattered light) with UV photons with energies ~2 eV. Before measurements, the samples were placed in a quartz cell with window and furnace sections connected to a vacuum line, calcined in static O_2 (6-10 kPa) at 723 K for 1 h, and finally outgassed (10^{-3} Pa) at 473 K for 1 h.

Photocatalytic liquid phase oxidation of 2-propanol by dissolved Oxygen

Before reaction, 50 mg of Ti_xSiBEA, previously calcined in static O_2 (6-10 kPa) at 723 K for 1 h and then outgassed (10^{-3} Pa) at 473 K for 1 h, were placed in a quartz tube with a 2-propanol aqueous solution (3.3×10^{-3} mol/L, 25 mL). Prior to UV-light irradiation, the suspension was stirred in a flow of O_2 for 10 min under dark conditions. The samples were irradiated for 55 h at 295 K using UV light from a 100W high-pressure Hg lamp (Toshiba SHLS-1002B) under stirring. The products were analyzed by on-line gas phase chromatography with flame ionization detector (FID) and Porapak Q column to separate the reactants from the products. The yield of acetone was calculated as follows:

$$\text{Yield of acetone (\%)} = ([\text{Acetone}]_t / [2-\text{Propanol}]_{t=0}) \times 100$$

where $[\text{Acetone}]_t$ is the concentration of acetone at time t and $[\text{2-propanol}]_{t=0}$ is the initial concentration of 2-propanol.

Photocatalytic gas phase oxidation of CO with N_2O

100 mg of Ti_xSiBEA, previously calcined in static O_2 (6-10 kPa) at 723 K for 1 h and then outgassed (10^{-3} Pa) at 473 K for 1 h, were placed in a quartz reactor. After introduction of the gaseous reactants (15 μmol of N_2O and CO), the quartz reactor was irradiated at 298 K

using UV light from a 100W high-pressure Hg lamp (Toshiba SHL-100UVQ-2) through a water filter for 1 h. The products were analyzed by on-line gas phase chromatography with thermal conductivity detector (TCD) and Molecular Sieve 5 A column for separation of N_2 and CO and Porapak Q column for separation of CO_2 and N_2O. The yields of CO_2 and N_2 were calculated as follows:

$$\text{Yield of } CO_2 \quad (\%) = (\text{ moles of } CO_2 / \text{ moles of } CO_{t=0}) \times 100$$

$$\text{Yield of } N_2 \quad (\%) = (\text{ moles of } N_2 / \text{ moles of } N2O_{t=0}) \times 100$$

where $CO_{t=0}$ and $N_2O_{t=0}$ are moles of CO and N_2O introduced at time t=0, respectively.

2.3. Results and Discussions

Figure 2.1 shows the XRD patterns of AlBEA, SiBEA, $Ti_{1.5}$SiBEA, $Ti_{3.2}$SiBEA and $Ti_{5.8}$SiBEA which all are typical of BEA zeolite. The crystallinity is preserved after dealumination and the samples do not show any evidence of extra lattice crystalline compounds or long-range amorphization of the zeolite. The decrease of the d_{302} spacing related to the narrow main diffraction peak near 22.6° from 3.942 Å (AlBEA; 2θ = 22.55°) to 3.912 Å (SiBEA; 2θ = 22.71°) upon dealumination indicates contraction of the matrix as a result of removal Al atoms, in line with earlier data [2,4,5,8]. In contrast, the significant increase from 3.912 Å (SiBEA) to 3.939, 3.941 and 3.942 Å (2θ = 22.66, 22.61 and 22.57°) upon introduction of 1.5, 3.2 and 5.8 Ti wt.% into SiBEA indicates expansion of the matrix, in a similar way as reported for VSiBEA zeolites [2,4]. The increase of the d_{302} spacing with Ti content is taken as evidence for the incorporation of Ti into the framework because the Ti–O bond distance (1.80 Å, for tetracoordinated Ti species) is longer than that of Si–O (typically 1.60–1.65 Å in zeolites) [16].

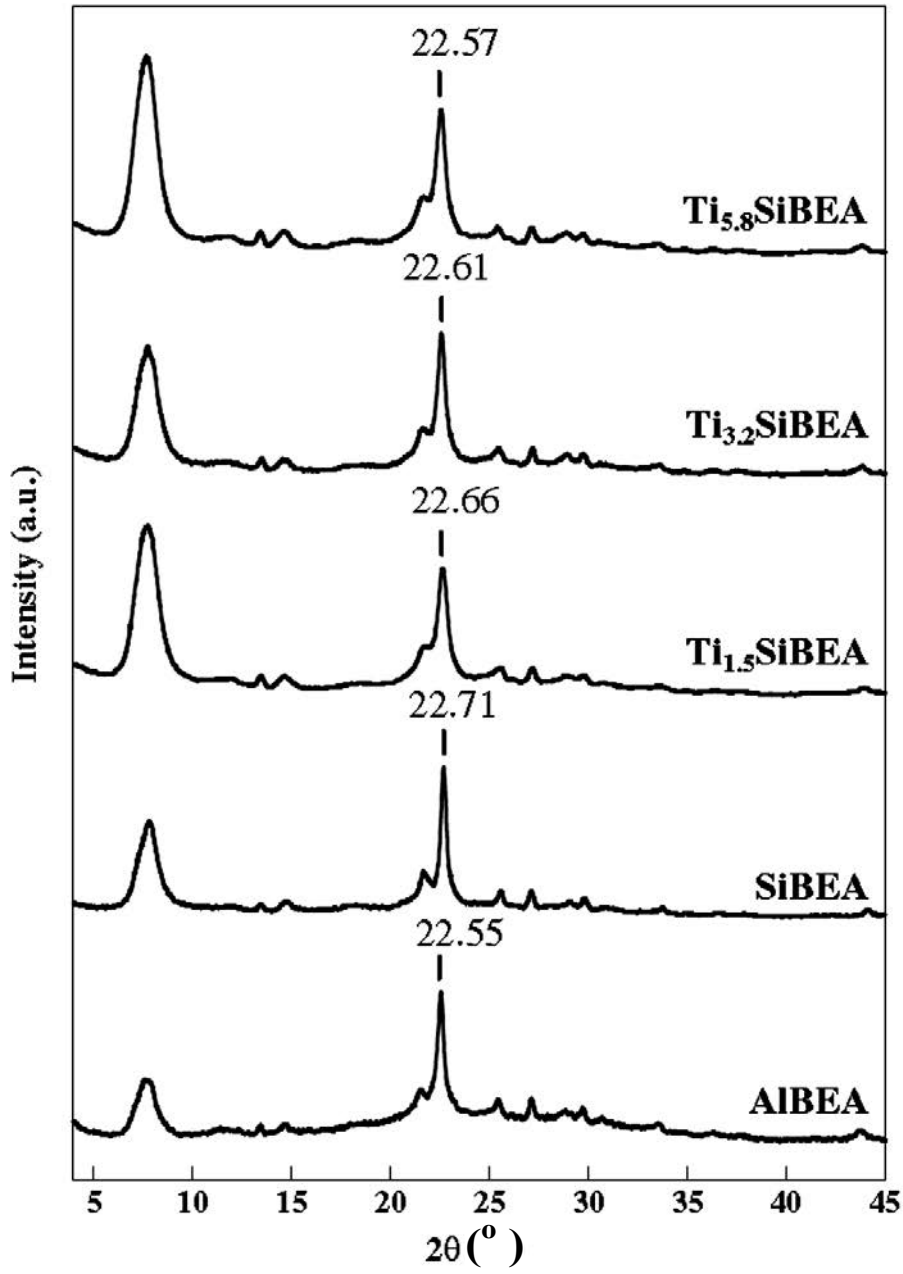

Figure 2.1 X-ray diffractograms recorded at ambient atmosphere of AlBEA, SiBEA, $Ti_{1.5}$SiBEA, $Ti_{3.2}$SiBEA and $Ti_{5.8}$SiBEA.

Moreover, after incorporation of Ti ions in SiBEA, the broad IR band at 3520 cm^{-1} due to H-bonded SiOH groups and the peak at ~−101 ppm in ^{29}Si-MAS NMR spectra assigned to Si atoms in a $Si(OH)(OSi)_3$ environment are less intense, confirming that $TiCl_4$ vapor has reacted with silanol groups, as reported earlier [8]. The DR UV–Vis spectra of Ti_xSiBEA zeolites exhibit two main bands at 220–230 and 265–290 nm assigned to oxygen to tetrahedral and octahedral Ti^{4+} charge transfer transitions, respectively, as reported earlier for TiSiBEA zeolites and TiMCM-41 [13,17]. As calculated on the basis of XPS results reported earlier, the amount of framework tetrahedral Ti^{4+} and octahedral Ti^{4+} increases from 1.3 to 3.1 and 0.2 to 2.7 %, respectively, for Ti content increasing from 1.5 to 5.8 wt.% [13].

Because of its high sensitivity to the local environment of transition metal ions photoluminescence spectroscopy can be used to investigate the nature of Ti species. Ti_xSiBEA zeolites excited at 270 nm exhibit emission spectra at 77 K with maxima at 430–470 nm (Figure 2.2) [1,3,17]. Similar spectra have been previously reported for titanium ions incorporated into the framework of Y zeolite [8,9]. The emission spectra correspond to transition from the excited triplet state $(Ti^{3+}–O)^*$, produced upon UV-light irradiation (270 nm) of Ti_xSiBEA at 298 K (Scheme 2.1), to the ground singlet state ($Ti^{4+}–O^{2-}$) of highly dispersed tetrahedral Ti species. When Ti_xSiBEA zeolites are irradiated by UV-light, the isolated tetrahedral Ti species produce the excited triplet state $(Ti^{3+}–O)^*$ with a lifetime long enough to allow the appearance of photoluminescence as a radiative decay to the ground state. The decrease in the photoluminescence intensity with increasing Ti content is probably due to the nonradiative deactivation of the photoluminescence arising from an efficient energy transfer to nearby Ti^{4+} ions, in tetrahedral and/or octahedral coordinations.

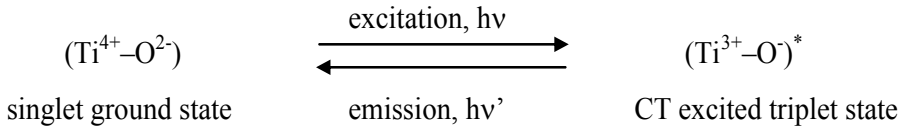

Scheme 2.1.

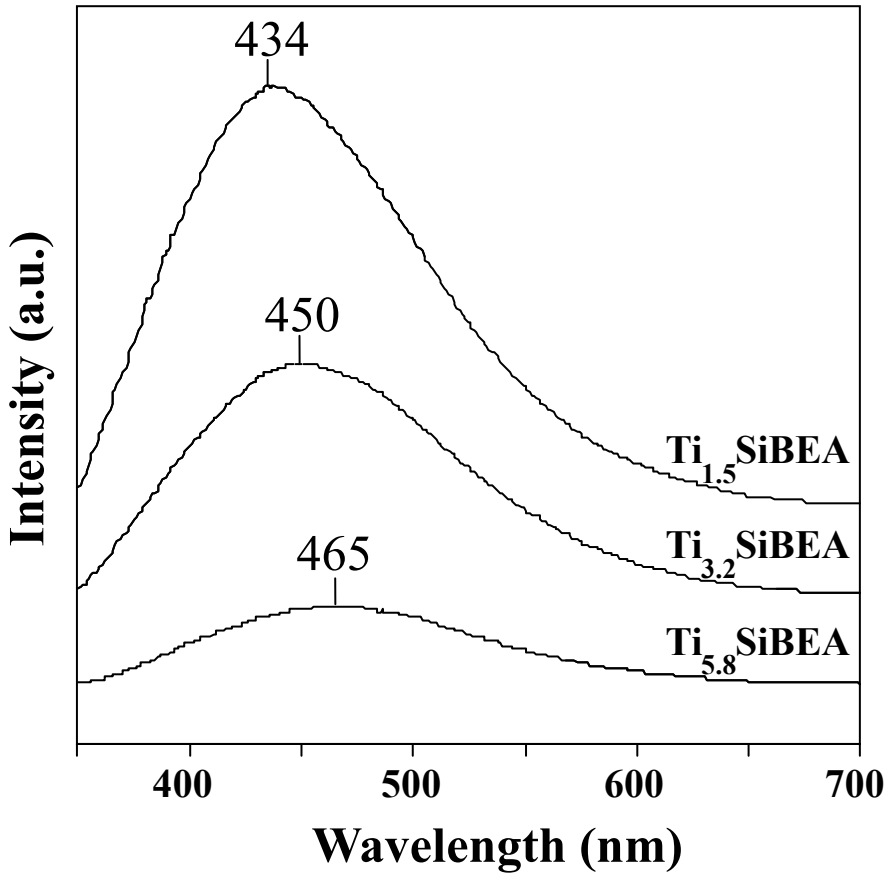

Figure 2.2 Photoluminescence spectra recorded at 77 K for Ti_xSiBEA zeolites previously calcined in static O_2 (6–10 kPa) at 723 K for 1 h and then outgassed (10^{-3} Pa) at 473 K for 1 h. Photoluminescence spectra were recorded with an excitation wavelength of 270 nm.

The photocatalytic activity of Ti_xSiBEA zeolites in the liquid phase oxidation of 2-propanol depends on the Ti content as shown by the different 2-propanol conversion plotted as a function of time (Figure 2.3). Indeed, the 2-propanol conversion is lowest for $Ti_{1.5}SiBEA$ and highest for $Ti_{3.2}SiBEA$, suggesting that there is an optimum Ti content to obtain a maximum 2-propanol conversion. Such a possibility is indicated by the data presented in Figure 2.1. The intensity of photoluminescence decreases with Ti content from 1.5 to 5.8 wt.% suggesting the existence of a maximum activity for some composition of Ti_xSiBEA zeolites. Further investigations of Ti_xSiBEA zeolites with Ti content intermediate between 1.5 and 3.2 wt.% are underway to precisely determine the role of Ti environment on the activity in 2-propanol oxidation. The yield of acetone increases with Ti content and reaches a value of ~50 % for 55 h of reaction on $Ti_{5.8}SiBEA$, as shown in Figure 2.4. The differences between the amounts 2-propanol converted and those of acetone produced over all the samples is related to the fact that 2-propanol is very probably oxidized not only into acetone but also into CO_2, as it has been previously reported on various TiO_2 catalysts [18]. It should be noted that formation of acetone is negligible under dark conditions (data not shown). The lower activity of $Ti_{1.5}SiBEA$ than that of $Ti_{3.2}SiBEA$ and $Ti_{5.8}SiBEA$ can be ascribed to the difference in the local structure of Ti^{4+} species. In fact, changes in the local structure of transition metal ions within the framework of BEA zeolite upon increasing metal content have been reported [15]. The decrease in acetone formation for Ti content above 3.2 wt.% is likely due to the formation of more amount of octahedral Ti^{4+} species which are less photocatalytically active than their tetrahedral analogues, as earlier reported [1,18]. We consider that the framework tetrahedral Ti^{4+} is main active site in Ti_xSiBEA as it is mention in our earlier work [13]. The amounts of the framework tetrahedral Ti^{4+} and octahedral Ti^{4+} in the $Ti_{3.2}SiBEA$ are 2.6 and 0.6 wt.%, respectively, as we have determined by XPS measurements and reported earlier [13]. While the amounts of the framework tetrahedral

Ti^{4+} and octahedral Ti^{4+} in the $Ti_{5.8}$SiBEA are 3.1 and 2.7 wt.%, respectively. Considering that the photocatalytic conversion of 2-propanol on $Ti_{3.2}$SiBEA and $Ti_{5.8}$SiBEA are similar (Figure 2.3), it can be concluded that the framework tetrahedral Ti^{4+} is the main active species in Ti_xSiBEA. The lower selectivity into acetone formation on tetrahedral Ti^{4+} species can be ascribed to their strong oxidation ability which enhances the further oxidation of acetone into CO_2. It seems that stronger oxidation ability of tetrahedral Ti^{4+} species than octahedral one is related to higher UV absorption energy (HOMO–LUMO energy gap) of tetrahedral Ti^{4+} species than that of octahedral one due to the quantum size effect, in line with earlier report [18].

The photocatalytic gas phase oxidation of CO with N_2O has been investigated on the same Ti_xSiBEA zeolites (Table 2.1). The activity depends on the Ti content, as shown by different CO and N_2O conversions for $Ti_{1.5}$SiBEA, $Ti_{3.2}$SiBEA and $Ti_{5.8}$SiBEA, with the values of 99% for CO and 100% for N_2O on $Ti_{3.2}$SiBEA and $Ti_{5.8}$SiBEA respectively and only 12% for CO and 4% for N_2O on $Ti_{1.5}$SiBEA (Table 1), in line with the results observed for 2-propanol oxidation. As shown in Table 1, for $Ti_{3.2}$SiBEA and $Ti_{5.8}$SiBEA photocatalysts, the CO_2 and N_2 yields are close to 100% suggesting that almost all CO is oxidized into CO_2 with stoichiometric conversion of N_2O into N_2. However, in the case of $Ti_{5.8}$SiBEA, the yield of CO_2 (103 %) is slightly higher than the conversion of CO (99 %). This result may be ascribed to the oxidation of organic contaminants adsorbed on the catalyst surface. It should be noted that photocatalytic gas phase oxidation of CO with N_2O hardly proceeds on SiBEA (Table 1) suggesting that the isolated tetrahedral species in the excited triplet state $(Ti^{3+}–O)^*$ within the framework of BEA structure plays a significant role in this reaction.

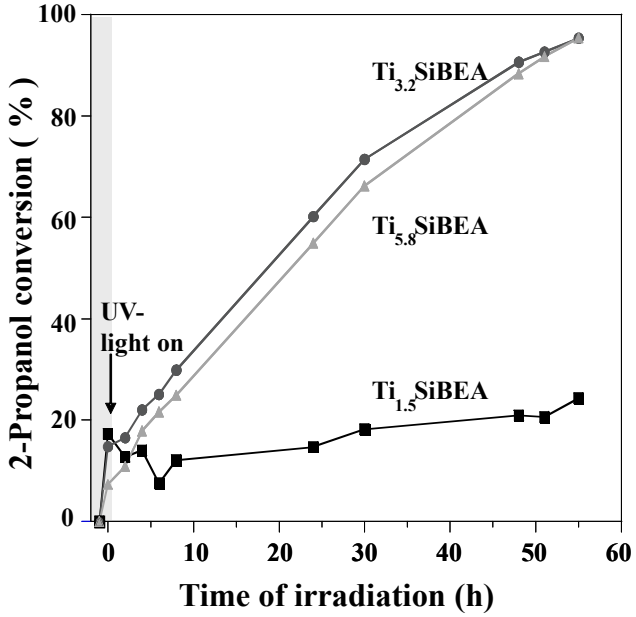

Figure 2.3 Conversion of 2-propanol vs time in the photocatalytic liquid phase oxidation of 2-propanol with dissolved O_2 performed at 298 K on Ti_xSiBEA zeolites previously calcined in static O_2 (6–10 kPa) at 723 K for 1 h and then outgassed (10^{-3} Pa) at 473 K for 1 h.

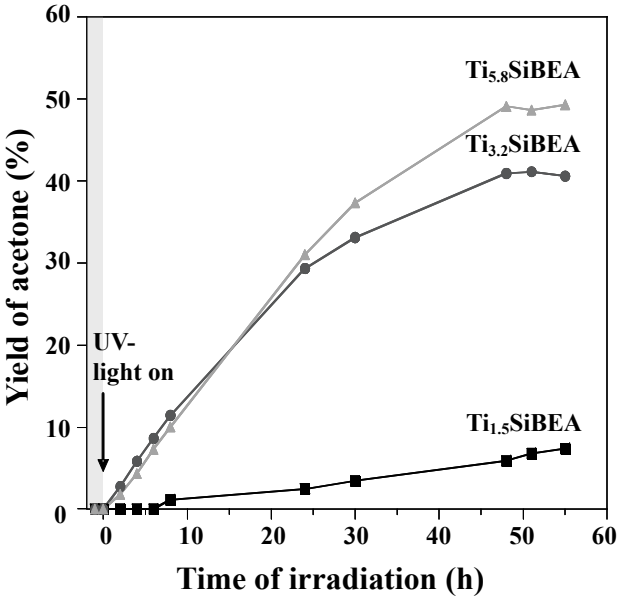

Figure 2.4 Yield of acetone vs time in the photocatalytic liquid phase oxidation of 2-propanol with dissolved O_2 performed at 298 K on Ti_xSiBEA zeolites previously calcined in static O_2 (6–10 kPa) at 723 K for 1 h and then outgassed (10^{-3} Pa) at 473 K for 1 h.

Table 2.1 CO and N_2O conversions and yields of CO_2 and N_2 in the photocatalytic oxidation of CO with N_2O performed at 298 K on SiBEA, $Ti_{1.5}$SiBEA, $Ti_{3.2}$SiBEA and $Ti_{5.8}$SiBEA previously calcined in O_2 (6–10 kPa) at 723 K for 1 h and then outgassed at 473 K for 1 h.

Material	**Conversions** (%)		**Yields** (%)	
	CO	**N_2O**	**CO_2**	**N_2**
SiBEA	9	1	0	0
$Ti_{1.5}$SiBEA	12	4	4	5
$Ti_{3.2}$SiBEA	100	100	99	96
$Ti_{5.8}$SiBEA	99	100	103	91

2.4. Conclusions

The present work evidences the influence of Ti content on the liquid phase oxidation of 2-propanol by dissolved oxygen and of the gas phase oxidation of CO by N_2O photocatalyzed by Ti_xSiBEA (x=1.5, 3.2 and 5.8 Ti wt.%) zeolites. The incorporation of Ti ions into the framework of zeolite is evidenced by the progressive increase of the d_{302} spacing with Ti content. DR UV–Vis and photoluminescence investigations show that mainly isolated tetrahedral Ti^{4+} species are present in $Ti_{1.5}$SiBEA and $Ti_{3.2}$SiBEA zeolites. They are active sites of oxidation of 2-propanol and CO and their photocatalytic activity depends on the Ti content as shown by different conversions of 2-propanol and CO for $Ti_{1.5}$SiBEA, $Ti_{3.2}$SiBEA and $Ti_{5.8}$SiBEA. The 2-propanol conversion is lowest for $Ti_{1.5}$SiBEA and highest for $Ti_{3.2}$SiBEA, suggesting that there is an optimum Ti content to obtain a maximum 2-propanol conversion. For these photocatalysts, the maximum yield of acetone is ~50 % and CO_2 and N_2 yields are close to 100. The data suggest that isolated tetrahedral Ti ions in their excited triplet state $(Ti^{3+}–O)^*$, produced upon UV-light irradiation of Ti_xSiBEA, play an important role in the photocatalytic oxidation of 2-propanol into acetone and of CO into CO_2.

2.5. References

[1] M. Anpo, M. Che, Adv. Catal., **44**, 119 (1999).

[2] S.Dzwigaj, M.J. Peltre, P. Massiani, A. Davidson, M. Che, T. Sen, S. Sivasanker, Chem. Commun., 87 (1998).

[3] M. Anpo, S. Dzwigaj, M. Che, Adv. Catal., **52**,1 (2009).

[4] S. Dzwigaj, P. Massiani, A. Davidson, M. Che, J. Mol. Catal., **155**, 169 (2000).

[5] S. Dzwigaj, M. Che, J. Phys. Chem. B, **110**, 12490 (2006).

[6] S. Dzwigaj, J. Janas, T. Machej, M. Che, Catal. Today **119**, 133 (2007).

[7] S. Dzwigaj, J. Janas, J. Mizera, J. Gurgul, R.P. Socha, M. Che, Catal. Lett., **126**, 36 (2008).

[8] J.P. Nogier, Y. Millot, P.P. Man, T. Shishido, M. Che, S. Dzwigaj, J. Phys. Chem., C, **113**, 4885 (2009).

[9] M. Anpo, M. Sunamoto, M. Che, J. Phys. Chem., **93**, 1187 (1989).

[10] M. Anpo, T.H. Kim, M. Matsuoka, Catal. Today ,**142**, 114 (2009).

[11] M. Takeuchi, S. Sakai, A. Ebrahimi, M. Matsuoka, M. Anpo, Top. Catal., **52**, 1651 (2009).

[12] Q.H. Xia, X. Chen, T. Tatsumi, J. Mol. Catal. A, **176**, 179 (2001).

[13] J.P. Nogier, Y. Millot, P.P. Man, C. Methivier, M. Che, S. Dzwigaj, Catal. Lett., **130**, 588 (2009).

[14] F. Chiker, J.P. Nogier, F. Launay, J.L. Bonardet, Appl. Catal. A, **259**, 153 (2004).

[15] S. Dzwigaj, M. Matsuoka, M. Anpo, M. Che, The J. Phys. Chem. B, **104**, 6012 (2000).

[16] T. Blasco, M.A. Camblor, A. Corma, P. Esteve, J.M. Guil, A. Martinez, J.A. Pedrigon-Melon, S. Valencia, J.Phys. Chem. B, **102**, 75 (1998).

[17] L. Marchese, T. Maschmeyer, E. Gianotti, S. Coluccia, J.M. Thomas, J. Phys. Chem. B, **101**, 8836 (1997).

[18] H. Yamashita, M. Honda, M. Harada, Y. Ichihashi, M. Anpo, T. Hirao, N. Itoh, N. Iwamoto, J. Phys. Chem. B, **102**, 10707 (1998).

Chapter 3

Synthesis and Application of Tin Triflate–Containing MCM-41 as Heterogeneous Lewis Acid Catalysts for Mukaiyama-Aldol Reaction at Room Temperature

3.1. Introduction

Lewis acid metal halides, such as $AlCl_3$, $FeCl_3$ and $ZnCl_2$, are most widely used as homogeneous catalysts for industrial organic synthesis because of their low cost and high availability. These acids also have some drawbacks which include followings: the use of the metal halides in stoichiometric or higher amounts, the generation of high amounts of aqueous effluents during the post-synthesis work-up and the difficulty of recovering and reusing of the catalysts from the effluent. To solve these issues, many researchers have focused on heterogeneous catalytic systems, enabling to recover the catalysts after the end of the reaction and to reuse them for further catalytic cycles. However, heterogeneous catalysts often show inferior performances compared to the homogenous ones under the same reaction conditions; therefore, the desired is the developments of highly active heterogeneous catalysts.

Recently, Corma et al. reported that Ti-containing mesoporous silica catalysts have high catalytic activity for heterogeneous Mukaiyama-aldol reactions [1]. Silica-based porous materials, such as mesoporous silicas and zeolites, are characterized by the high specific surface area, chemical resistance and easiness to incorporate various metal species [1-7]. Therefore, these porous materials are often used as catalyst support. As compared to Ti^{4+} ions, Sn^{4+} ions incorporated in MFI type zeolites are noticed to be more acidic and show higher catalytic activity in cyclohexanol dehydration reaction [7]. However, the strong Lewis acid sites are easily deactivated in water by hydration [8]. In this context, Kobayashi et al. revealed that homogeneous metal triflate catalysts can be used as Lewis acid-catalyzed reactions in the presence of water [8-10]. This water tolerance of Lewis acid catalysts are due to less-nucleophilicity of their triflate (OTf) ligands. Thus, the Sn-containing silica-based porous material catalysts are expected to show an enhanced Lewis acid catalytic activity by coordination of Sn^{4+} with OTf ligands.

In this study, Sn-containing MCM-41 with different content of tin (Sn_x-MCM-41; x = 1.4,

5.5 and 6.7 wt.%) were prepared by a hydrothermal synthesis method and were subsequently treated with triflic acid to form tin triflate within the silica framework (Sn_xOTf-MCM-41) by following the methods reported by Coman et al. and co-workers [11-14]. Sn_xOTf-MCM-41 were used in a Mukaiyama-aldol reaction of benzaldehyde with 1-trimethylsiloxy cyclohexene at room temperature as a model Lewis acid-catalyzed reaction. Moreover, FT–IR analyses using pyridine as a probe molecule were carried out for the evaluation of acid sites.

3.2. Experimental

Synthesis of Sn_xOTf-MCM-41

Sn_xOTf-MCM-41 were prepared via the synthesis of Sn_x-MCM-41 followed by a triflic acid treatment. Firstly, Sn_x-MCM-41 with tin content of 1.4, 5.5 and 6.7 wt.% were synthesized by a hydrothermal method [3,15]. A given amount of $SnCl_4$•$5H_2O$ was dissolved in 15 mL of distilled water and mixed with 16.7 g of cetyltrimethylammonium chloride (CTMACl) as structure template. After CTMACl was dissolved, 2.08 g of tetramethylammonium hydroxide and 12.5 mL of distilled water were added. Then, 13.6 g of tetramethylammonium silicate was added dropwise to the solution, which was stirred for 20 min. Furthermore, 3.1 g of fumed silica was added slowly to the above solution, and the obtained suspension was stirred for 1 h. The resulting mixture was transferred to a stainless-steel autoclave and aged in an oven at 393 K for 5 days under static conditions to complete the crystallization. The resulting product was filtered off, washed with distilled water and dried at 373 K for 12 h followed by calcination at 823 K for 8 h in air to remove the residual structure template, yielding Sn_x-MCM-41 as white powder. Subsequently, Sn_x-MCM-41 were treated in a triflic acid solution [11-14]. Typically, 2.0 g of Sn_x-MCM-41 was stirred under reflux at 353 K for 15 h in a triflic acid solution (5.0 g of triflic acid in 50

mL of methanol). The resulting white powdered sample was collected by filtration, washed with methanol adequately to eliminate excess triflic acid on the silica surface and dried at 353 K for 12 h. The obtained samples were designated as Sn_xOTf-MCM-41 (x = 1.4, 5.5 and 6.7 wt.%).

Characterization of Sn_xOTf-MCM-41

X-ray diffraction (XRD) patterns were collected by a Shimadzu XRD-6100 using Cu Kα radiation (λ = 1.5406 Å). Diffuse reflectance UV–Vis spectra were obtained using a Shimadzu UV-2200A spectrophotometer. FT–IR spectra were recorded with a resolution of 4 cm^{-1} in a transmission mode using a JASCO FT–IR 660 Plus. For the measurements, samples were pressed into self-supported disks (1 cm^2, 12 mg/cm). *In-situ* FT–IR experiments were also carried out by using pyridine as molecular probe for the evaluation of acid properties. Prior to measurements, the sample disks were degassed at 373 K for 2 h in vacuo and treated with saturated pyridine vapor at room temperature for 30 min followed by evacuation at 373 K for 30 min to remove the physisorbed pyridine. The pyridine-adsorbed FT–IR spectra were then collected at room temperature. The difference spectra were obtained by subtracting reference spectra collected before pyridine adsorption.

Heterogeneous Mukaiyama-aldol reaction

The heterogeneous Mukaiyama-aldol reactions of benzaldehyde with 1-trimethylsiloxy cyclohexene were carried out in a glass vessel equipped with a vacuum line connector. The 30 mg of catalyst was placed in the glass vessel and pre-treated at 373 K for 2 h in vacuo. After replacement to Ar atmosphere, 5.0 mL of dry-toluene, 1.0 mmol of benzaldehyde and 1.2 mmol of 1-trimethylsiloxy cyclohexene were added in the glass vessel. The reaction was carried out at room temperature for 3 h under stirring. After the reaction, 0.33 mmol of

9-methylanthracene was added to the reaction mixture as an index for ^{1}H-NMR. The catalyst and toluene were removed by filtration and evaporation, respectively. The analyses of substances were performed by ^{1}H-NMR.

3.3. Results and Discussions

The XRD patterns of Sn_xOTf-MCM-41 and a pure silica MCM-41 are given in Figure 3.1. All diffraction patterns were almost the same as those of MCM-41 materials reported by Beck et al. [2]. A sharp diffraction peak was observed at $2\theta = 2–2.5°$ in all patterns, which is ascribed to the (100) reflection of a hexagonal structure of mesopores. Besides the strong peak, these patterns show the weak diffraction peaks at $3^o < 2\theta < 7^o$ ascribed to (110), (200) and (210) reflections of the mesopores. In addition, the surface area of $Sn_{5.5}$-MCM-41 and $Sn_{5.5}$OTf-MCM-41, determined by N_2 adsorption-desorption isotherms, were 1107 and 924 m^2/g, respectively. These results reveal that the mesoporous structure was retained even after the incorporation of tin triflate into the MCM-41 frameworks. The observable peak shift to higher angle with increase in tin content implies that the pore size became narrower due to larger ionic radius of Sn^{4+} compared to Si^{4+}. On the other hand, no diffraction peaks ascribed to tin compounds, such as crystalline tin oxide, were observed in the higher angle region. This finding shows that the Sn species within the silica framework exist in highly dispersed states without formation of aggregated species.

Diffuse reflectance UV–Vis spectroscopy is a very sensitive probe for the detection of the coordination state of Sn species [15-16]. It is also ideal technique to verify the incorporation of tin in the MCM-41 structure. Figure 3.2 shows the UV–Vis diffuse reflectance spectra of Sn_xOTf-MCM-41. For comparison, the spectra of bulk SnO_2 and pure silica MCM-41 are also included in Figure 3.2. The bulk SnO_2 spectrum exhibits a broad absorption at around 284 nm assigned to hexacoordinated polymeric Sn–O–Sn type species [15-16], while the

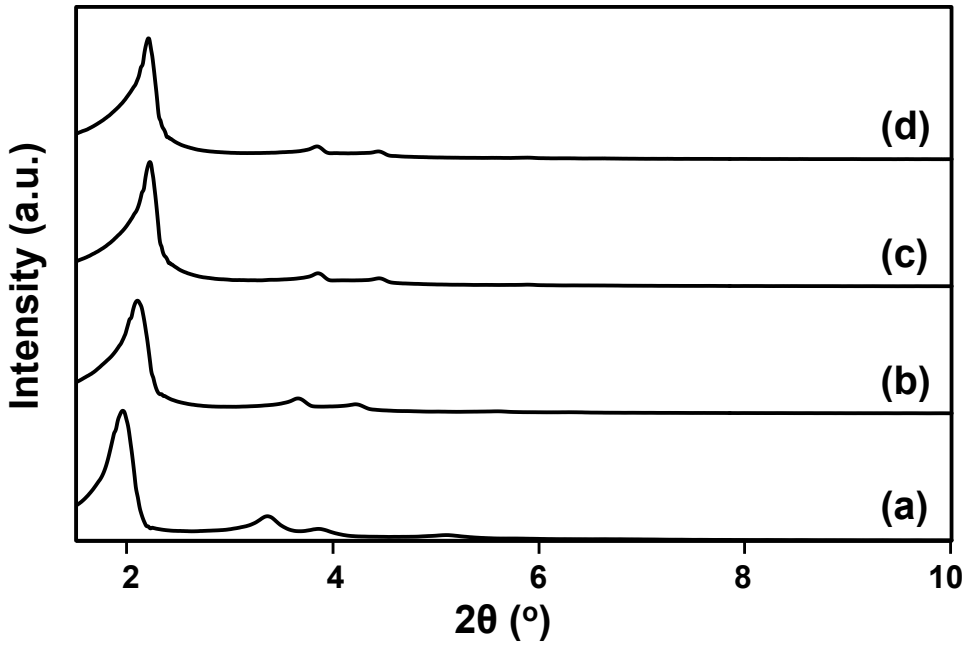

Figure 3.1 XRD patterns of (a) MCM-41 and (b–d) Sn_xOTf-MCM-41 with tin content of (b) 1.4, (c) 5.5 and (d) 6.7 wt.%.

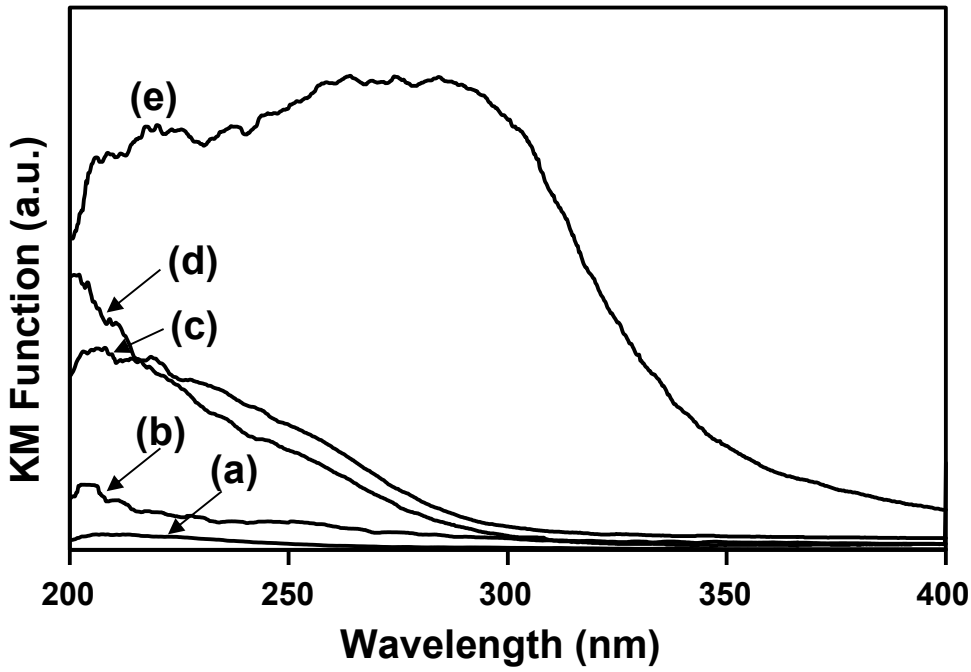

Figure 3.2 Diffuse reflectance UV–Vis spectra of (a) MCM-41, (b–d) Sn_xOTf-MCM-41 with tin content of (b) 1.4, (c) 5.5 and (d) 6.7 wt.% and (e) SnO_2.

MCM-41 exhibits almost no absorption band in this range. The spectra of all Sn_xOTf-MCM-41 showed absorption band at around 208 nm, suggesting the presence of Sn^{4+} in tetrahedral coordination within their silica frameworks of Sn_xOTf-MCM-41 [15-16]. In addition, the peak intensity at around 208 nm was found to increase with increasing the content of tin in Sn_xOTf-MCM-41. However, the broader character of the peak from 208 to 300 nm may be associated with the presence of site-isolated Sn species in a distorted tetrahedral environment and in penta- or octahedral coordination sphere [15].

Figure 3.3 shows FT–IR spectra of $Sn_{5.5}$-MCM-41 and a pure silica MCM-41 before and after trifliric acid treatments. The FT–IR spectrum of tin triflate is also included in Figure 3.3 as a reference compound. $Sn_{5.5}$-MCM-41 and MCM-41 spectra clearly exhibited vibrational bands of ν_{as}(Si–O–Si), ν_s(Si–O–Si) and δ(Si–O–Si) at 1085, 800 and 455 cm^{-1}, respectively [17-18]. After trifliric acid treatments, $Sn_{5.5}$OTf-MCM-41 gave new vibration bands at 1269, 1210 and 785 cm^{-1} attributed to CF_3 vibrations and at 1179, 1035 and 645 cm^{-1} attributed to S=O and S–O vibrations, respectively, which were coincident with the spectrum of tin triflate [19]. These results suggest that tin triflate is successfully formed within the porous silica frameworks by the post-synthesis triflic acid treatment. In contrast, no significant change was observed in the spectrum of pure silica MCM-41 even after triflic acid treatment. These findings indicate that the OTf ligands are selectively coordinated with Sn sites in the Sn_x-MCM-41.

In an investigation exploring the potential catalytic activities of Sn_x-MCM-41 and Sn_xOTf-MCM-41, heterogeneous Mukaiyama-aldol reaction of benzaldehyde with 1-trimethylsiloxy cyclohexene was performed at room temperature (Scheme 3.1). Mukaiyama-aldol reactions are catalyzed by Lewis acids and allow for the reaction of an aldehyde with a silyl enolate [1]. As shown in Table 3.1, Sn_x-MCM-41 and Sn_xOTf-MCM-41 showed catalytic activity for the Mukaiyama-aldol reaction and gave the

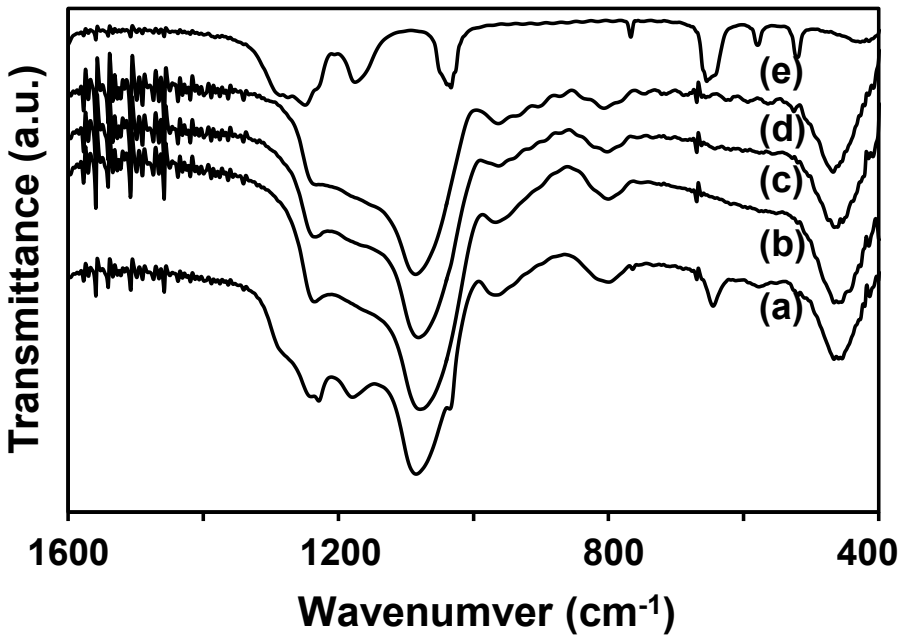

Figure 3.3 FT–IR spectra of (a, b) $Sn_{5.5}$-MCM-41 and (c, d) MCM-41 before (b, d) and after (a, c) trifliric acid treatments and (e) tin triflate.

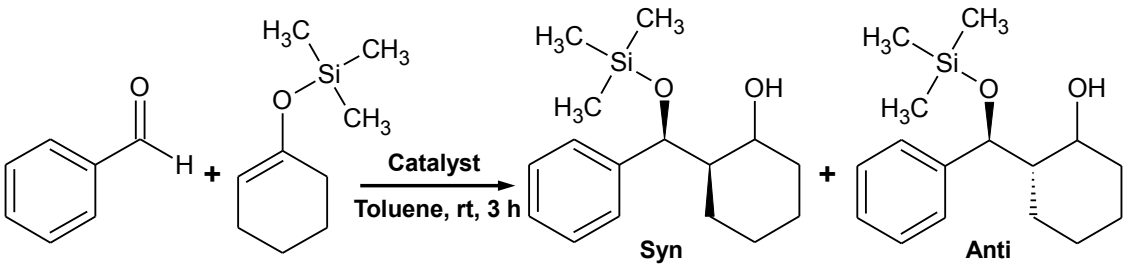

Scheme 3.1

Table 3.1 Mukaiyama-aldol reaction of benzaldehyde with 1-trimethylsiloxy cyclohexene using various solid acid catalysts.

Entry	Catalyst	Sn content / wt%	Yield[a] / %	TON[b]	Selectivity / %	
					Syn	Anti
1	Sn-MCM-41	1.4	1.2	3.4	100	0
2	Sn-MCM-41	5.5	27.5	19.8	98	2
3	Sn-MCM-41	6.7	31.5	18.5	98	2
4	SnOTf-MCM-41	1.4	4.5	12.8	85	15
5	SnOTf-MCM-41	5.5	57.8	42.2	97	3
6	SnOTf-MCM-41	6.7	58.5	34.4	97	3
7	Sn-MCM-41[c]	5.5	55.6	40.1	98	2
8	$Sn(OTf)_2$/MCM-41	5.5	59.4	42.9	50.6	49.4
9	MCM-41	-	n.d.	-	-	-
10	SnO_2	78.8	n.d.	-	-	-

a) Yield of aldol products, b) Turn over number (TON) = [moles of aldol products] / [mole of Sn in the catalyst], c) Pre-treated at 573 K for 2 h in vacuo before the use in the reaction.

syn-product with high selectivity, while bulk SnO_2 and pure silica MCM-41 hardly promoted this reaction under the same reaction conditions. The yields of products increased with increasing the tin content in Sn_x-MCM-41 and Sn_xOTf-MCM-41. However, TON of $Sn_{6.7}$-MCM-41 and $Sn_{6.7}$OTf-MCM-41 catalysts were lower than those of catalysts with tin content of 5.5 wt.%. This would be because the ratio of tetrahedrally coordinated Sn species acting as a Lewis acid site decreases with increase in the tin content above 5-6 wt.% within Sn_x-MCM-41 and Sn_xOTf-MCM-41. Thus, the optimal content of tin is determined to be around 5.5 wt.%. Furthermore, Sn_xOTf-MCM-41 exhibited much higher catalytic activity than Sn_x-MCM-41, indicating that the Lewis acid property of tetrahedrally coordinated Sn species can be enhanced by the coordination of Sn^{4+} with OTf ligands. Interestingly, $Sn_{5.5}$-MCM-41 pre-treated at a high temperature of 573 K for 2 h in vacuo before the use in the reaction showed a similar catalytic activity to $Sn_{5.5}$OTf-MCM-41 (entry 7). Considering that the pre-treatment helps to remove adsorbed water molecules that suppress Lewis acid property from Lewis acid sites, coordinating OTf ligands should play a role in preventing the adsorption of water molecules on tetrahedrally coordinated Sn species. On the other hand, MCM-41-supported $Sn(OTf)_2$ ($Sn(OTf)_2$/MCM-41, 5.5 wt.% Sn), which was prepared by an impregnation method using an ethanol solution of $Sn(OTf)_2$ and MCM-41, showed no syn/anti selectivity (entry 8). This finding indicates that the presence of tetrahedrally coordinated Sn species is responsible for high syn selectivity.

To gain an insight into the detailed reason for the enhancement of catalytic ability, *in-situ* FT–IR experiments were carried out using pyridine as a probe molecule for acid sites. The pyridine adsorption technique is adopted for the assessment of Brönsted and Lewis acidities [20]. Figure 4 shows the difference FT–IR spectra of pyridine-adsorbed MCM-41, $Sn_{5.5}$-MCM-41 and $Sn_{5.5}$OTf-MCM-41. In the spectra acquisition, the sample disks were degassed at 373 K for 2 h in vacuo before pyridine adsorption. For comparison,

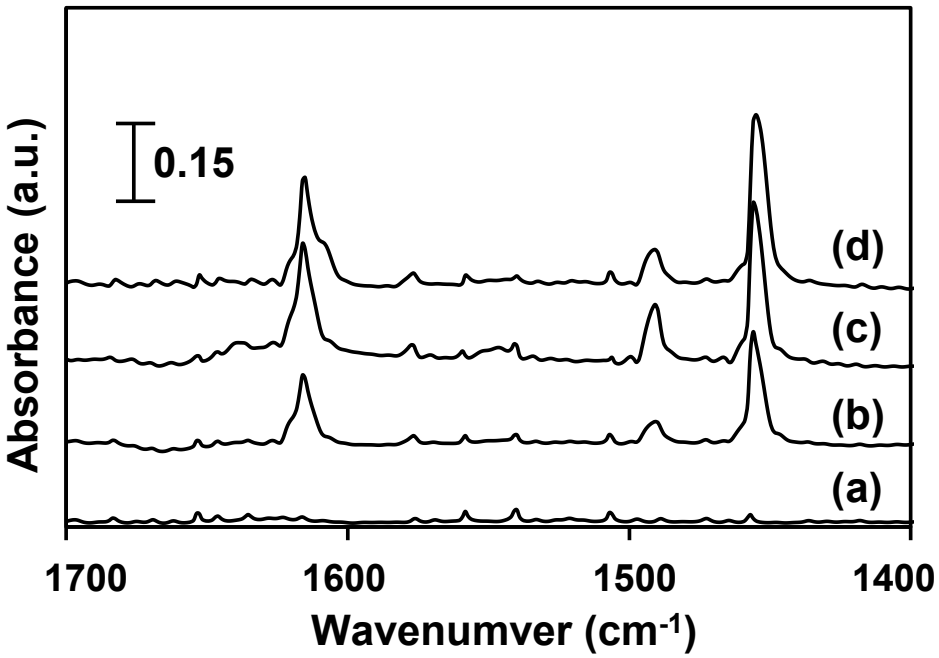

Figure 3.4 Difference FT–IR spectra of pyridine adsorbed on (a) MCM-41, (b) $Sn_{5.5}$-MCM-41 and (c) $Sn_{5.5}$OTf-MCM-41 pre-treated at 373 K before pyridine adsorption and (d) $Sn_{5.5}$-MCM-41 pre-treated at 573 K before pyridine adsorption.

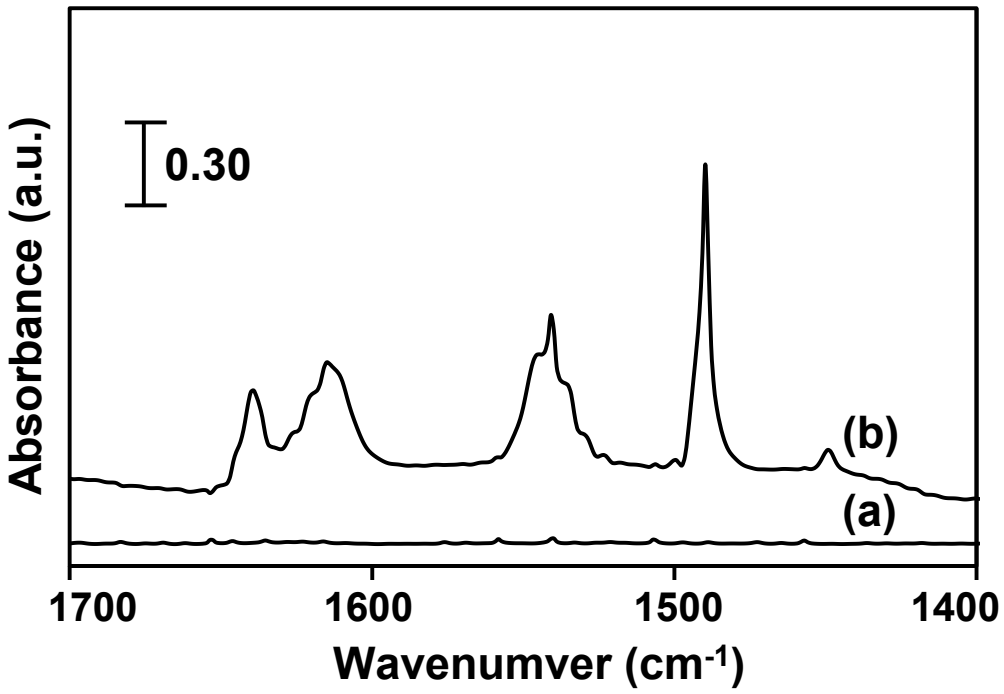

Figure 3.5 Difference FT–IR spectra of pyridine adsorbed on (a) MCM-41 and (b) $Sn(OTf)_2$/MCM-41.

$Sn_{5.5}$-MCM-41 pretreated at 573 K for 2 h in vacuo is also shown. The $Sn_{5.5}$-MCM-41 and $Sn_{5.5}$OTf-MCM-41 exhibited typical bands at around 1455 and 1616 cm^{-1} assigned to the adsorbed pyridine on Lewis acid sites, while MCM-41 exhibited no absorption band in this range. These results indicate that the Lewis acid sites are formed by the incorporation of Sn species. Additionally, the intensity of peaks at 1455 and 1616 cm^{-1} in the $Sn_{5.5}$OTf-MCM-41 spectrum were higher than those in $Sn_{5.5}$-MCM-41 and nearly the same as those in $Sn_{5.5}$-MCM-41 pretreated at 573 K. This result suggests that $Sn_{5.5}$OTf-MCM-41 possesses a great number of effective Lewis acid sites even at a low pre-treatment temperature of 373 K, which is consistent with the results of the catalytic reaction. In the homogeneous systems, the metal salt of triflic acid or metal triflates fall into an interesting category of catalysts having high water tolerance and the possibility to fix them on supports [21]. Therefore, it is considered that the coordinating OTf ligands would bring about water tolerance to tetrahedrally coordinated Sn species as Lewis acid sites. Taking into account the fact that the number of Lewis acid sites in $Sn_{5.5}$OTf-MCM-41 is equal to that in $Sn_{5.5}$-MCM-41 pretreated at 573 K, almost all Lewis acid sites in $Sn_{5.5}$OTf-MCM-41 should be protected from adsorption of water molecules due to the coordinating OTf ligands, that is, tetrahedrally coordinated Sn species should be coordinated with at least one OTf ligand. Furthermore, it is worth noting that $Sn(OTf)_2$/MCM-41 exhibited typical bands at around 1640 and 1540 cm^{-1} assigned to the adsorbed pyridine on Brönsted acid sites and at around 1455 and 1616 cm^{-1} assigned to the adsorbed pyridine on Lewis acid sites, as shown in Figure 3.5. This result implies that $Sn(OTf)_2$/MCM-41 possesses not only Lewis acid sites but also Brönsted acid sites and the Brönsted acid sites may account for its low selectivity. The detailed studies on reaction mechanisms are now under way.

Finally, the reusability of the $Sn_{5.5}$OTf-MCM-41 catalyst for the heterogeneous Mukaiyama-aldol reaction was investigated under the same reaction conditions. The

recovering of catalyst was performed by filtration from the reaction mixture and drying at 373 K for 4 h in air. As shown in Figure 6, $Sn_{5.5}$OTf-MCM-41 exhibited almost the same catalytic activity until 3 catalytic cycles, suggesting that the tin triflates were stably incorporated within the mesoporous silica framework without leaching during the reactions.

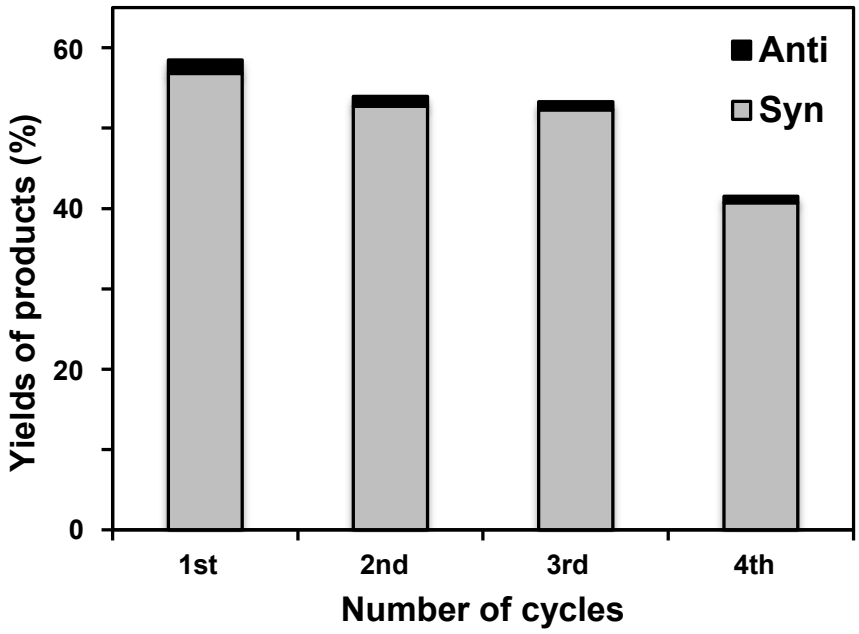

Figure 3.6 Mukaiyama-aldol reaction of benzaldehyde with 1-trimethylsiloxy cyclohexene over $Sn_{5.5}$OTf-MCM-41 and recycling results.

3.4. Conclusions

The tin triflate-containing MCM-41 with different content of tin (Sn_xOTf-MCM-41; x = 1.4, 5.5 and 6.7 wt.%) were successfully prepared by a two-step synthesis method. In the first step, Sn-containing mesoporous silicas (Sn_x-MCM-41) were prepared by a conventional hydrothermal method. Subsequently, the obtained Sn_x-MCM-41 were treated with triflic acid to form tin triflate within the silica frameworks. The characterization studies revealed that the synthesized Sn_xOTf-MCM-41 possessed highly ordered mesoporous structures and that the OTf ligands were selectively coordinated with Sn species in tetrahedral coordination

within their silica frameworks. Sn_xOTf-MCM-41 exhibited higher catalytic activity for Mukaiyama-aldol reaction of benzaldehyde with 1-trimethylsiloxy cyclohexene, as compared to Sn_x-MCM-41. This enhancement is attributed to the increase in the number of effective Lewis acid sites due to the coordination of Sn^{4+} with OTf ligands, in which the OTf ligands would bring about water tolerance to tetrahedrally coordinated Sn species. Furthermore, the $Sn_{5.5}OTf$-MCM-41 catalyst could be reused in the Mukaiyama-aldol reaction at least 3 times.

3.5. References

[1] R. Garro, M.T. Navarro, J. Primo, A. Corma, J. Catal. **233**, 342 (2005).

[2] J.S. Beck, J.C. Vartulli, W.J. Roth, M.E. Leonowicz, C.T. Kresge, K.D. Schmitt, C.T-W. Chu, D.H. Olson, E.W. Sheppard, S.B. McCullen, J.B. Higgins, J.L. Schlenker, J. Am. Chem. Soc. **114**, 10834 (1992).

[3] T.K. Das, K. Chaudhari, A.J. Chandwadkar, S. Sivasanker, J. Chem. Soc. Chem. Commun. 2495 (1995).

[4] R. Kumar, P. Vincent, K.V. Srinivasan, V.N. Raju, M. Sasidharan, Chem. Commun. 129 (1996).

[5] M. Sasidharan, R. Kumar, Catal. Lett. **38**, 251 (1996).

[6] M. Sasidharan, R. Kumar, J. Catal. **220**, 326 (2003).

[7] N.K. Mal, A.V. Ramaswamy, J. Mol. Catal. A Chem. **105**, 149 (1996).

[8] S. Kobayashi, I. Hachiya, J. Org. Chem. **59**, 3590 (1994).

[9] K. Manabe, Y. Mori, T. Wakabayashi, S. Nagayama, S. Kobayashi, J. Am. Chem. Soc. **122**, 7202 (2000).

[10] S. Kobayashi, K. Manabe, Acc. Chem. Res. **35**, 209 (2002).

[11] S.M. Coman, G. Pop, C. Stere, V.I. Parvulescu, J.E. Haskouri, D. Beltran, P. Amoros, J. Catal. **251**, 388 (2007).

[12] N. Candu, S.M. Coman, V.I. Parvulescu, J.E. Haskouri, P. Amoros, D. Beltran, Top. Catal. **52**, 571 (2009).

[13] V.I. Parvulescu, S.M. Coman, N. Candu, J.E. Haskouri, D. Beltran, P. Amoros, J. Mater. Sci. **44**, 6693 (2009).

[14] M. Verziu, J.E. Haskouri, D. Beltran, P. Amoros, D. Macovei, N. G. Gheorghe, C.M. Teodorescu, S.M. Coman, V.I. Parvulescu, Top. Catal. **53**, 763 (2010).

[15] T.R. Gaydhankar, P.N. Joshi, P. Kalita, R. Kumar, J. Mol. Catal. A Chem. **265**, 306 (2007).

[16] K. Chaudhari, T.K. Das, P.R. Rajmohanan, K. Lazar, S. Sivasanker, A. Chandwadkar, J. Catal. **183**, 281 (1999).

[17] M.D. Alba, Z.H. Luan, J. Klinowski, J. Phys. Chem. **100**, 2178 (1996).

[18] C.A. Koh, R. Nooney, S. Tahir, Catal. Lett. **47**, 199 (1997).

[19] L.E. Fernandez, A.B. Altabef, E.L. Varetti, Spectrochim. Acta A, **52**, 287 (1996).

[20] S. Endud, K.L. Wong, Micropor. Mesopor. Mater. **101**, 256 (2007).

[21] E. Altman, G.D. Stefanidis, T.V. Gerven, A. Stankiewicz, Ind. Eng. Chem. Res. **51**, 1612 (2012).

Chapter 4

Construction of Organoruthenium Complexes (–[biphRuCp]PF_6–) within Biphenylene–Bridged Inorganic–Organic Hybrid Mesoporous Materials and Their Catalytic Activities for Selective Hydrosilylation of 1-Hexyne

4.1. Introduction

Inorganic–organic hybrid mesoporous materials (HMMs) also known as periodic mesoporous organosilicas have attracted attention in the fields of adsorbents, sensors and light harvesting or emitting optical devices [1-13]. Various organic moieties (–C_2H_4–, –C_6H_4–, –$(C_6H_4)_2$–, etc.) covalently embedded within HMM structures are readily available for the post-synthetic introduction of unique functional sites [11-19]. For example, Inagaki et al. have achieved the development of solid acid and base catalysts by the introduction of sulfuric acid and amino groups, respectively, into organic moieties of HMMs [16-19]. Moreover, the organic moieties, particularly phenylene moieties, of HMMs can be utilized as ‘‘framework ligands’’ that directly coordinate to metal centers of organometallic complexes [20,21].

In our previous work, an organoruthenium complex (–[phRuCp]PF_6–; ph = –C_6H_4–, Cp = cyclopentadienyl) was successfully constructed within phenylene–bridged HMM (HMM–ph) by a simple ligand exchange reaction between $[(CH_3CN)_3RuCp]PF_6$ and phenylene moiety of HMM–ph [22]. In this complex, the metal center is directly coordinated with phenylene moiety of HMM–ph that behave as a “framework ligand”, enabling the complex to be present in high dispersion on HMM–ph [18,19]. As a consequence, the constructed organoruthenium complex exhibits excellent catalytic activities for selective hydrosilylation of 1-hexyne. Chemical properties of organic moieties within HMMs that can behave as framework ligands are expected to affect the catalytic performance of the constructed organometallic complexes; therefore, investigations of the effect of the kinds of framework ligands on catalytic performance of such organoruthenium complexes are of significant interest.

Herein, we focused on biphenylene–bridged HMM (HMM–biph; biph = –$(C_6H_4)_2$–) and attempted to construct an organoruthenium complex (–[biphRuCp]PF_6–) on the biphenylene moiety by a simple ligand exchange reaction (Scheme 1). The thus-synthesized HMM–

biphRuCp was characterized in detail by XRD, UV–Vis and XAFS techniques. In order to evaluate the effect of the kinds of framework ligands on the catalytic performance, HMM–biphRuCp and HMM–phRuCp were applied as catalysts for selective hydrosilylation of 1-hexyne with triethylsilane in a solid–gas heterogeneous system.

4.2. Experimental

Synthesis of HMM–biphRuCp

HMM–biph was prepared according to a procedure reported by Inagaki et al. [11,23,24]. 2.5 mmol of 4,4'-bis(triethoxysilyl)biphenyl [$(C_2H_5O)_3Si–(C_6H_4)_2–Si(OC_2H_5)_3$] was added into a mixture of octadecyltrimethylammonium chloride (C_{18}TMACl) surfactant, 30.4 mmol of 6.0 N sodium hydroxide, and 3.3 mmol of distilled water, under vigorous stirring at ambient temperature. The suspension was stirred for another 20 h and then heated at ca. 368 K for 22 h under static conditions. The resulting precipitate was recovered by filtration and was washed with deionized water. Finally, the surfactant was removed from the obtained powder sample by extraction with a mixture of 150 mL of ethanol and 3.1 g of 2.0 M HCl aqueous solution at ambient temperature for 8 h. Subsequently, the –[biphRuCp]PF_6– complexe was constructed within HMM–biph by a ligand exchange reaction by using $CHCl_3$ solution of $[(CH_3CN)_3RuCp]PF_6$. Typically, 58 mg of $[(CH_3CN)_3RuCp]PF_6$, which was synthesized in two steps from readily available bis-benzeneruthenium(II) chloride, was dissolved in 20 mL of dry-$CHCl_3$. 400 mg of HMM–biph pretreated at 473 K for 2 h in vacuum was then added in the above obtained orange colored solution [25,26]. After refluxing for 24 h under Ar atmosphere, the white powdered sample was recovered by filtration, repeatedly washed with $CHCl_3$, and then dried in vacuum, yielding HMM–biphRuCp. For comparison purposes, HMM–phRuCp was also prepared by the same method except for using 1,4-bis(triethoxysilyl)benzene [$(C_2H_5O)_3Si–C_6H_4–Si(OC_2H_5)_3$].

Characterization of HMM–biphRuCp

X-ray diffraction (XRD) patterns were collected by a Shimadzu XRD-6100 using Cu Kα radiation (λ = 1.5406 Å). Diffuse reflectance UV–Vis spectra were obtained using a Shimadzu UV-2200A spectrophotometer. The Ru K-edge X-ray absorption fine structure (XAFS) spectra were also recorded at the BL-01B1 facility of SPring–8 at the Japan Synchrotron Radiation Research Institute (JASRI). All spectra were recorded in fluorescence mode with a Si(111) two-crystal monochromator at 298 K. The extended X-ray absorption fine structure (EXAFS) data were examined using an analysis program (Rigaku REX2000). In order to obtain the radial structure function, Fourier transformations of k^3–weighted EXAFS oscillations in the range of 3–12 $Å^{-1}$ were performed.

Selective hydrosilylation of 1-hexyne with triethylsilane

The selective hydrosilylation reactions of 1-hexyne with triethylsilane were performed in a solid–gas heterogeneous system at 523 K for 15 h in a closed system (cell volume: 80 mL). Typically, 30 mg of catalyst was placed in the reaction cell and pre-treated at 473 K for 3 h in vacuo. Then, 527 μmol of 1-hexyne and triethylsilane were added to the reaction cell using vacuum line. The reactions were carried out at 523 K for 15 h. The resulting substances were collected by liquid N_2, diluted by 2.0 mL of $CHCl_3$ and then analyzed by gas chromatograph using a Shimadzu GC–14B with a flame ionization detector equipped with an InertCap® 1 capillary column.

4.3. Results and Discussions

Figure 4.1 shows XRD patterns of the synthesized HMM–ph and HMM–biph. In both XRD patterns, a sharp diffraction peak was observed at 2θ = 2.0° (d = 44 Å) corresponding to

the (100) reflection of a hexagonal structure of mesopores [23,24]. HMM–ph exhibited the other three peaks in the range of 2θ = 10–40° (d = 7.6, 3.8 and 2.5 Å) derived from the periodicity of phenylene and silica layers (*i.e.*, $O_{1.5}$–Si–C_6H_4–Si–$O_{1.5}$ units) with a spacing of 7.6 Å in the pore wall [11]. On the other hand, HMM–biph exhibited five peaks in the range of 2θ = 6–40° (d = 11.6, 5.9, 3.9, 2.9 and 2.4 Å) derived from the periodicity of biphenylene and silica layers (*i.e.*, $O_{1.5}$–Si–C_6H_4–C_6H_4–Si–$O_{1.5}$ units) with a spacing of 11.6 Å in the pore wall [23,24]. This difference in the periodicity is due to the difference in the length of organic moieties, that is, longer biphenylene moieties than phenylene ones lead to the increase in the interval of the periodicity. These results reveal that phenylene or biphenylene units were successfully embedded in the periodic mesoporous structures.

Subsequently, UV–Vis measurements were performed to verify the construction of the –[biphRuCp]PF_6– complex within the framework of HMM–biph [22]. Figure 4.2 shows diffuse reflectance UV–Vis spectra of HMM–biph before and after ligand exchange reaction. UV–Vis absorption spectra of [C_6H_6RuCp]PF_6 and [$(CH_3CN)_3$RuCp]PF_6 complexes dissolved in CH_3CN as reference compounds are also shown in the inset of Figure 4.2. The spectrum of [$(CH_3CN)_3$RuCp]PF_6 in CH_3CN exhibited an absorption band at 370 nm with a tail extending into the visible region, while [C_6H_6RuCp]PF_6 in CH_3CN exhibited an absorption band assigned to *d–d* transition in only UV-wavelength region. It was found that the synthesized HMM–biph exhibited no absorption bands above 330 nm. On the other hand, a new absorption band was observed in the range of 300–400 nm after the ligand exchange reaction. The position of the new band was identical to that of *d–d* transition band of the [C_6H_6RuCp]PF_6 complex (λ = ~325 nm), indicating that a similar complex to [C_6H_6RuCp]PF_6 was formed through the ligand exchange reaction between [$(CH_3CN)_3$RuCp]PF_6 and biphenylene moiety of HMM–biph [27,28]. Similarly, the spectrum of HMM–phRuCp exhibited an absorption band at around 325 nm showing the construction of the

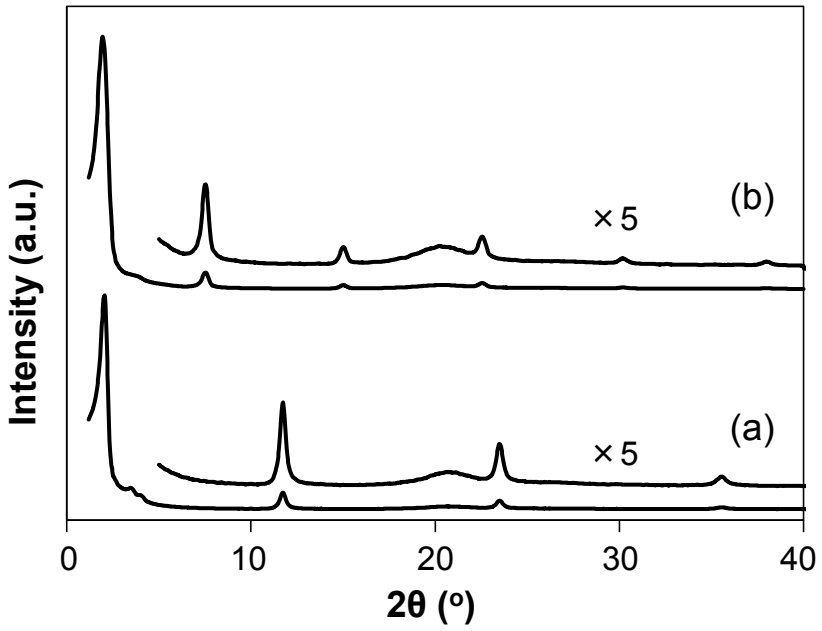

Figure 4.1 XRD patterns of (a) HMM–ph and (b) HMM–biph.

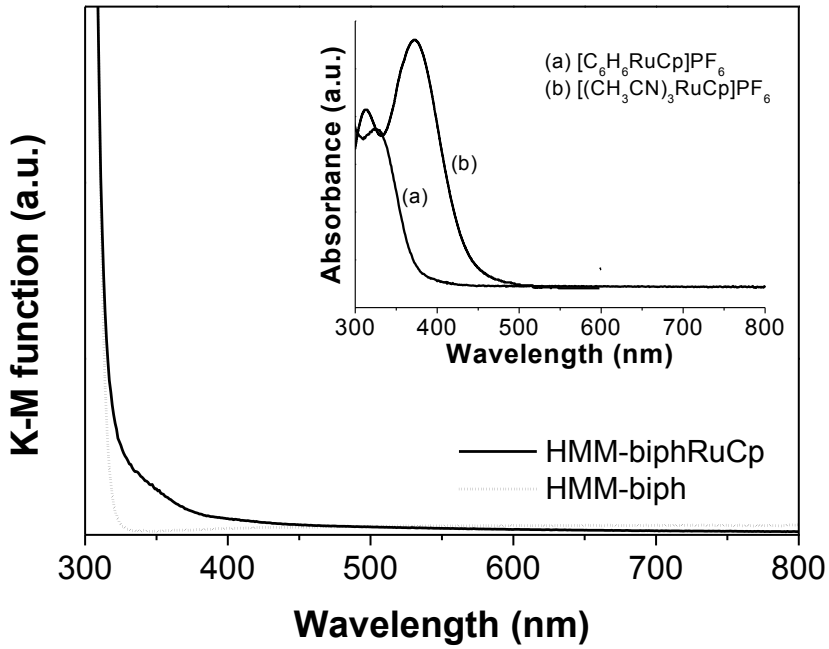

Figure 4.2 Diffuse reflectance UV–Vis spectra of HMM–biph (dotted line) and HMM–biphRuCp (solid line). Inset shows UV–Vis absorption spectra of (a) $[C_6H_6RuCp]PF_6$ and (b) $[(CH_3CN)_3RuCp]PF_6$ in CH_3CN.

–[phRuCp]PF_6– complex within HMM–ph [22]. These findings revealed that this ligand exchange reaction is an effective method to construct –[biphRuCp]PF_6– and –[phRuCp]PF_6– complexes within HMMs containing arene moieties.

To gain an insight into the local structures of –[phRuCp]PF_6– and –[biphRuCp]PF_6– complexes constructed within HMM–phRuCp and HMM–biphRuCp, respectively, Ru K-edge XAFS measurements were performed. Figure 4.3 shows XANES and Fourier transform of EXAFS (FT-EXAFS) spectra of HMM–phRuCp and HMM–biphRuCp, together with those of [C_6H_6RuCp]PF_6 and [$(CH_3CN)_3$RuCp]PF_6. The edge positions and spectral shapes, particularly in the region of white line, in XANES spectra of HMM–phRuCp and HMM–biphRuCp corresponded well to those in the [C_6H_6RuCp]PF_6 spectrum. This result strongly suggests that –[phRuCp]PF_6– and –[biphRuCp]PF_6– complexes were constructed within respective frameworks of HMM–ph and HMM–biph by direct coordination of ruthenium centers with phenylene moieties in their frameworks.

In the FT–EXAFS data, all spectra displayed a strong sharp peak at ca. 1.7 Å (without phase-shift correction) assigned to Ru–C or Ru–N bonds; however, the curve fitting analyses of EXAFS spectra revealed the difference in their coordination environments (Table 1). In the case of HMM–phRuCp and HMM–biphRuCp, the strong sharp peak was able to be assigned to bonds between ruthenium atom and neighboring carbon atoms of phenylene (C_{ph}) and cyclopentadienyl (C_{Cp}) ligands. Their bond lengths were determined to be Ru–C_{ph} = 2.23 Å (coordination number (CN) = 6.2) and Ru–C_{Cp} = 2.17 Å (CN = 5.2) for HMM–phRuCp and Ru–C_{Cp} = 2.23 Å (CN = 6.1) and Ru–C_{Cp} = 2.18 Å (CN = 5.1) for HMM–biphRuCp. These values were in good agreement with bond lengths of [C_6H_6RuCp]PF_6 (Ru–C_{ph} = 2.24 Å (CN = 6.0), Ru–C_{Cp} = 2.18 Å (CN = 5.1)). Meanwhile, the curve fitting analysis for [$(CH_3CN)_3$RuCp]PF_6 revealed the existence of Ru–N bonding (2.1 Å, CN = 3.4) and Ru–C_{Cp} bonding (2.16 Å, CN = 5.5), which were different from those in HMM–phRuCp

Table 4.1 The results of curve fitting analyses of EXAFS spectra of various catalysts.

Catalyst	Shell	R[a)] (Å)	CN[b)]
HMM–phRuCp	Ru–C_{ph}	2.23	6.2
	Ru–C_{Cp}	2.17	5.2
HMM–biphRuCp	Ru–C_{ph}	2.23	6.1
	Ru–C_{Cp}	2.18	5.1
$[C_6H_6RuCp]PF_6$	Ru–C_{ph}	2.24	6.0
	Ru–C_{Cp}	2.18	5.1
$[(CH_3CN)_3RuCp]PF_6$	Ru–N	2.10	3.4
	Ru–C_{Cp}	2.16	5.5

[a)]Bond distance, [b)]Coordination number

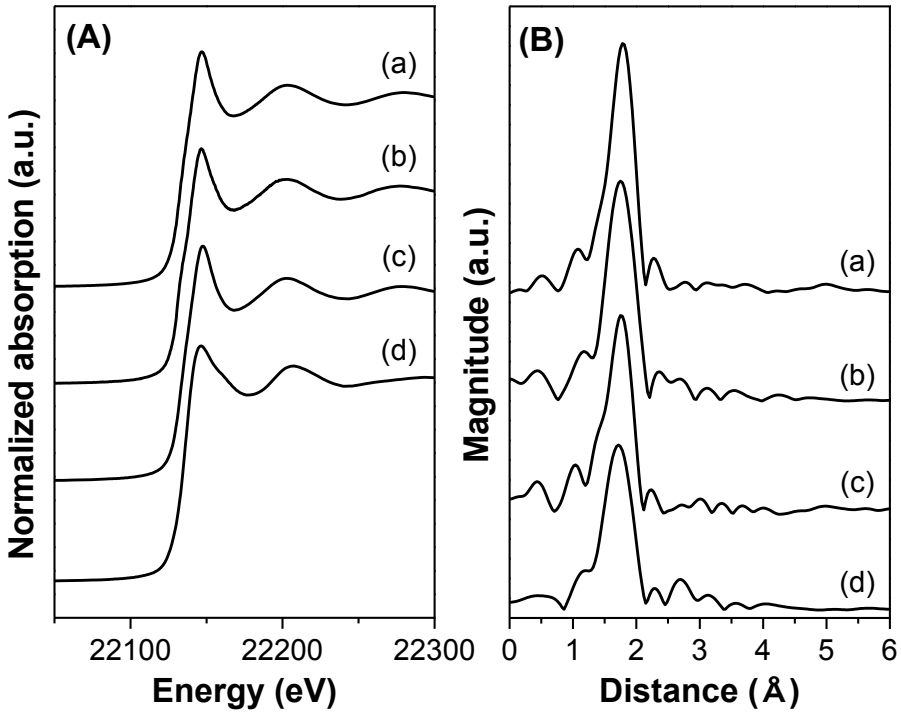

Figure 4.3 Ru K-edge (A) XANES and (B) Fourier transform of EXAFS spectra of (a) HMM–phRuCp, (b) HMM–biphRuCp, (c) $[C_6H_6RuCp]PF_6$ and (d) $[(CH_3CN)_3RuCp]PF_6$.

and HMM–biphRuCp. These results provide evidence that –[phRuCp]PF_6– and –[biphRuCp]PF_6– complexes are constructed within HMM–ph and HMM–biph frameworks through the ligand exchange reactions from $[(CH_3CN)_3RuCp]PF_6$. Furthermore, no other peaks were observed in the ranges of 2.0–3.0 Å assigned to Ru–Ru bond, indicating that aggregated species and dimeric ruthenium complexes are not contained in the HMM–phRuCp and HMM–biphRuCp [29,30].

The XANES data also provide information on the amount of Ru complexes loaded. Based on the peak intensity of white line, the amounts of –[phRuCp]PF_6– and –[biphRuCp]PF_6– complexes loaded were determined to be 1.1 wt% and 1.7 wt% of Ru metal, respectively. This difference will be derived from higher electron donating ability of biphenylene moieties than that of phenylene ones, because arene ligands bearing electron donating substituents can stabilize CpRu complexes [31]. Following the successful formation of –[phRuCp]PF_6– and –[biphRuCp]PF_6– complexes within HMMs, selective hydrosilylation of 1-hexyne with triethylsilane was performed in a solid–gas heterogeneous system at 523 K. It can be seen in Figure 4.4 that $[C_6H_6RuCp]PF_6$, HMM–phRuCp and HMM–biphRuCp exhibited catalytic activities for the hydrosilylation reaction and gave α-vinylsilane with high selectivity. In contrast, HMM–ph and HMM–biph exhibited almost no catalytic activities under the same reaction conditions. These results clearly indicate that –[phRuCp]PF_6– and –[biphRuCp]PF_6– complexes act as catalysts for the selective hydrosilylation reaction. Considering the fact that $[C_6H_6RuCp]PF_6$ does not show the catalytic activity for hydrosilylation reaction in a solid–liquid heterogeneous system at 298 K (data not shown), coordinatively unsaturated sites on the Ru(II) center would be formed by the thermal activation of –[phRuCp]PF_6– and –[biphRuCp]PF_6– complexes at 523 K. It was also found that $[C_6H_6RuCp]PF_6$ showed lower catalytic activity than HMM-phRuCp and HMM-biphRuCp. This lower catalytic activity would be associated with the aggregation of

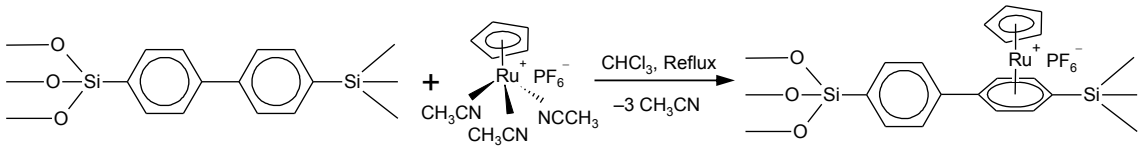

Scheme 4.1

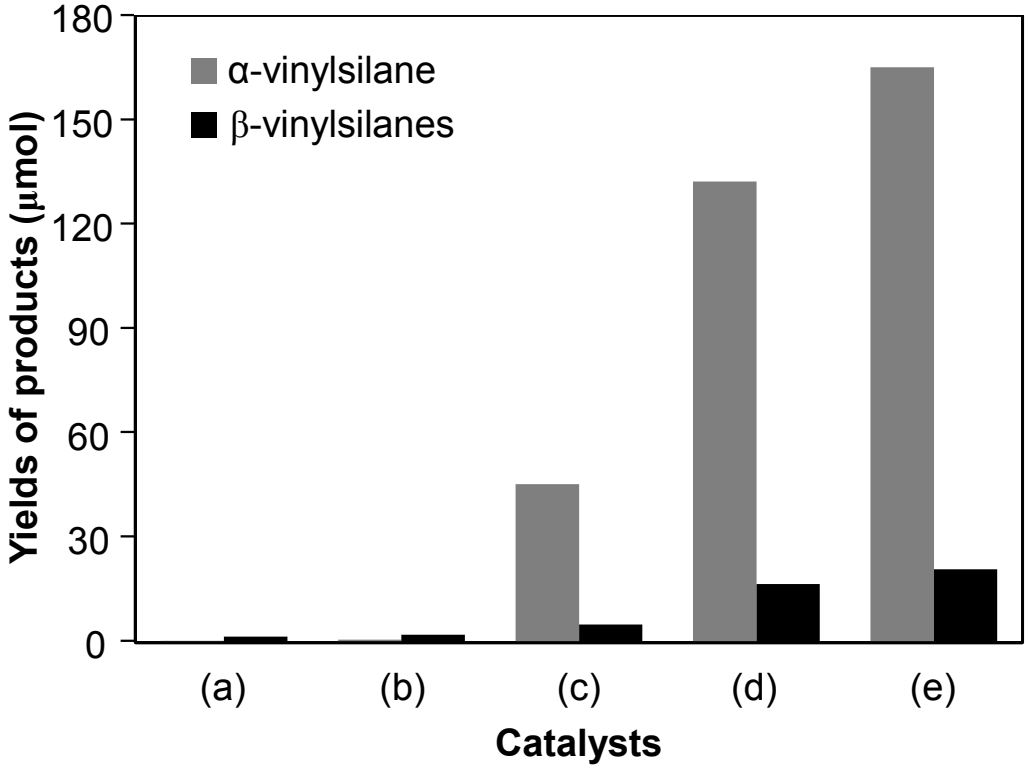

Figure 4.4 Yields of products for selective hydrosilylation of 1-hexyne with triethylsilane on (a) HMM–ph, (b) HMM–biph, (c) $[C_6H_6RuCp]PF_6$, (d) HMM–phRuCp and (e) HMM–biphRuCp. Reaction conditions: 1-hexyne and triethylsilane (527 μmol), catalyst (30 mg), 15 h, 523 K.

complexes, that is, the ligand exchange reaction allowed the immobilization of –[phRuCp]PF_6– and –[biphRuCp]PF_6– complexes onto HMMs in high dispersion states, resulting in the improvement of catalytic activities. Moreover, it was found that HMM–biphRuCp exhibited higher catalytic activity than HMM–phRuCp when compared on the basis of weight of catalysts used for the reaction. This would be due to the higher loading amount of the Ru complex derived from the electron donating ability of biphenylene moieties. Thus, it is demonstrated that organic moieties within HMMs that behave as framework ligands have an influence on chemical properties, herein stability, of the constructed complexes on them, resulting in the change in their catalytic activities.

4.4. Conclusions

The construction of the –[biphRuCp]PF_6– complex within HMM–biph was achieved through a ligand exchange reaction between [$(CH_3CN)_3$RuCp]PF_6 and biphenylene moiety of HMM–biph. UV–Vis and XAFS studies revealed that the constructed –[biphRuCp]PF_6– complex was present in the highly dispersed state within the HMM-biph framework without forming aggregated and dimeric ruthenium species. HMM–biphRuCp catalyzed selective hydrosilylation of 1-hexyne in a solid–gas heterogeneous system and gave α-vinylsilane as a main product. It was also found that HMM–biphRuCp exhibited higher catalytic activity than HMM–phRuCp. This high catalytic activity of HMM–biphRuCp was due to the higher loading amount of the Ru complex into HMM–biph derived from the electron donating ability of biphenylene moieties.

4.5. References

[1] S. Inagaki, S. Guan, Y. Fukushima, T. Ohsuna , O. Terasaki, J. Am. Chem. Soc., **121**, 9611 (1999).

[2] B.J. Melde, B.T. Holland, C.F. Blanford , A. Stein, Chem. Mater., **11**, 3302 (1999).

[3] T. Asefa, M.J. MacLachlan, N. Coombs , G.A. Ozin, Nature, **402**, 867 (1999).

[4] C. Yoshina-Ishii, T. Asefa, N. Coombs, M.J. MacLachlan , G.A. Ozin, Chem. Commun., 2539 (1999).

[5] F. Hoffmann, M. Cornelius, J. Morell , M. Fröba, Angew. Chem., Int. Ed., **45**, 3216 (2006).

[6] S. Fujita , S. Inagaki, Chem. Mater., **20**, 891 (2008).

[7] A. Stein, B.J. Melde , R.C. Schroden, Adv. Mater., **12**, 1403 (2000).

[8] A. Sayari, S. Hamoudi, Y. Yang, I.L. Moudrakovsk , J.R. Ripmeester, Chem. Mater., **12**, 3857 (2000).

[9] M. P. Kapoor, Q. Yang , S. Inagaki, J. Am. Chem. Soc., **124**, 15176 (2002).

[10] M. Cornelius, F. Hoffmann , M. Fr€oba, Chem. Mater., **17**, 6674 (2005).

[11] S. Inagaki, S. Guan, T. Ohsuna , O. Terasaki, Nature, **416**, 304 (2002).

[12] T. Tani, N. Mizoshita , S. Inagaki, J. Mater. Chem., **19**, 4451 (2009).

[13] S. Inagaki, O. Ohtani, Y. Goto, K. Okamoto, M. Ikai, K. Yamanaka, T. Tani , T. Okada, Angew. Chem., Int. Ed., **48**, 4042 (2009).

[14] J. G. Nguyen , S.M. Cohen, J. Am. Chem. Soc., **132**, 4560 (2010).

[15] S. Aguado, J. Canivet, Y. Schuurman, D. Farrusseng, J. Catal., **284**, 207 (2011).

[16] Q. Yang, J. Liu, J. Wang, M.P. Kapoor, S. Inagaki , C. Li, J. Catal., **228**, 265 (2004).

[17] K. Nakajima, I. Tomita, M. Hara, S. Hayashi, K. Domen , J.N. Kondo, Adv. Mater., **17**, 1839 (2005).

[18] M. Ohashi, M. P. Kapoor , S. Inagaki, Chem. Commun., 841 (2008).

[19] R. Voss, A. Thomas, M. Antonietti , G. A. Ozin, J. Mater. Chem., **15**, 4010 (2005).

[20] T. Kamegawa, T. Sakai, M. Matsuoka , M. Anpo, J. Am. Chem. Soc., **127**, 16784 (2005).

[21] M. Matsuoka, T. Kamegawa, T.H. Kim, T. Sakai , M. Anpo, J. Nanosci. Nanotechnol., **10**, 314 (2010).

[22] T. Kamegawa, M. Saito, T. Watanabe, K. Uchihara, M. Kondo, M. Matsuoka , M. Anpo, J. Mater. Chem., **21**, 12228 (2011).

[23] M.P. Kapoor, Q. Yang, S. Inagaki, J. Am. Chem. Soc., **124**, 15176 (2002).

[24] Y. Yang , A. Sayari, Chem. Mater., **20**, 2980 (2008).

[25] R.A. Zelonka , M.C. Baird, J. Organomet. Chem., **44**, 383 (1972).

[26] F. Grepioni, G. Cojazzi, D. Braga, E. Marseglia, L. Scaccianoce , B.F.G. Johnson, J. Chem. Soc., Dalton Trans., 553 (1999).

[27] T.P. Gill , K.R. Mann, Organometallics, **1**, 485 (1982).

[28] A.M. Mcnair, J.L. Schrenk , K.R. Mann, Inorg. Chem., **23**, 2633 (1984).

[29] E.E. Karslyan, A.I. Konovalov, D.S. Perekalin, P.V. Petrovskii , A.R. Kudinov, Russ. Chem. Bull., Int. Ed., **57**, 2201 (2008).

[30] Y. Nakajima , H. Suzukia, Organometallics, **22**, 959 (2003).

[31] D.S. Perekalin, E.E. Karslyan, P.V. Pertovskii, A.O. Borissova, K.A. Lyssenko , A.R. Kudinov, Eur. J. Inorg. Chem., 1485-1492 (2012).

Chapter 5

Enhanced Catalytic Activity of Arenetricarbonyl Chromium Complexes Constructed within Zr-Based MOFs by Introducing Substituents into Organic Linkers of the MOFs

5.1. Introduction

The metal–organic frameworks (MOFs) having a 3–dimensional network structures constructed from organic linkers and metal-oxo clusters have attracted attention in the fields of catalysts, adsorbents and separation materials owing to their extremely large surface areas and pore volumes and structural diversity that enables rational material design [1-5]. The functionalization of MOFs by introducing substituent groups, such as $–NH_2$ and $–SO_3H$ groups, into their organic linkers is a promising technique to control their chemical properties and to form catalytically active sites for organic synthesis [6,7]. For example, the control of adsorption characteristics and the development of acid or base catalysts by the introduction of varied substituent groups have hitherto been reported [6,7]. More recently, a unique methodology for functionalizing benzene rings within MOFs has been developed by Kaye et al. [8]. In this method, organochromium complexes are constructed within MOF frameworks by the direct coordination of chromium center with benzene rings belonging to the organic linker of MOFs [8,9]. Similar techniques have also been employed for the immobilization of organometallic complexes on inorganic–organic hybrid mesoporous material.

Molecular organometallic complexes often act as excellent catalysts showing high activity and selectivity for various organic syntheses. However, they are confronted with the difficulty in separation and recovery from reaction mixtures; therefore, much effort has been devoted to the immobilization of them onto support materials in order to use as reusable catalysts. Organometallic complexes constructed within MOF frameworks are expected to show not only reusability but also remarkable catalytic properties comparable to molecular organometallic complexes because of their closely similar coordination environments to molecular ones. However, yet few studies have targeted the application of such organometallic complexes constructed within MOFs to heterogeneous catalysts [10].

In this context, the present study deals with the development of heterogeneous arenetricarbonyl chromium ([–ArCr(CO)$_3$–]) complex catalysts constructed within Zr-based MOFs. Moreover, the effect of the introduction of substituents into organic linkers of the MOFs on the catalytic activity is described and discussed.

5.2. Experimental

Synthesis of Zr-based MOFs

A Zr-based MOF named UiO-66 was prepared by a conventional solvothermal method [11]. Terephthalic acid (1.64 mmol) and zirconium tetrachloride (1.80 mmol) were dissolved in N,N-dimethylformamide (DMF) (211 mL) and stirred for few minutes at room temperature. The mixture was placed in a Teflon-lined stainless-steel autoclave and heated in oven at 393 K for 24 h. After cooling to room temperature, the precipitate was filtered, washed repeatedly with DMF and dried at room temperature for 24 h. The obtained white powder sample was then dried under vacuum at 473 K for 2 h to remove residual DMF, yielding UiO-66 without substituents (UiO-66-H). In order to investigate the effect of substituents, a bromine-functionalized UiO-66 (UiO-66-Br) and amino-functionalized UiO-66 (UiO-66-NH_2) were prepared by the same procedure, except for using 2-bromo terephthalic acid and 2-amino terephthalic acid, respectively, in place of terephthalic acid [12].

Construction of [–ArCr(CO)$_3$–] complexes within Zr-based MOFs

[–ArCr(CO)$_3$–] complexes were constructed within Zr-based MOFs (UiO-66-X; X = H, Br or NH_2) by a chemical vapor deposition (CVD) technique with chromium hexacarbonyl ($Cr(CO)_6$) as a starting material [9,13-15]. Prior to CVD treatments, Zr-based MOFs were degassed at 473 K for 1 h to remove the adsorbed water molecules on their surfaces. Then, the Zr-based MOFs were subject to $Cr(CO)_6$ vapor at 393 K for 3 h in vacuo. Finally,

unreacted and physisorbed $Cr(CO)_6$ was removed by evacuation at 423 K for 3 h, yielding UiO-66-X-$Cr(CO)_3$.

Characterization of [–ArCr(CO)$_3$–] complexes within Zr-based MOFs

XRD (X-ray diffraction) data were recorded on a Shimadzu XRD-6100 using Cu Kα radiation (λ = 1.5406 Å). Nitrogen adsorption isotherms were measured at 77 K using a vacuum line with a mercury column. All the samples were degassed at 423 K for 3 h prior to data collection. The specific surface areas were calculated from the N_2 adsorption isotherm using the BET (Brunauer-Emmett-Teller) equilibrium equation. TPD (temperature-programed desorption) profiles were obtained by using a quadrupole mass spectrometer (Anelva M–QA100TS) connected with a vacuum line. FT–IR (Fourier–transform infrared spectroscopy) data were recorded with a Jasco FT–IR-660 plus.

Catalytic dehydrochlorination reaction

The dehydrochlorination of 2-chloro-2-methylbutane ($(CH_3)_2C(Cl)CH_2CH_3$) was performed in a solid–gas reaction system. The catalyst (90 mg) and degassed 2-chloro-2-methylbutane (0.3 mL) were charged into a glass vessel equipped with a vacuum line connector and heated at 358 K in an oven. At this temperature, 2-chloro-2-methylbutane and the reaction products exist in gaseous form. After heating for 22 h, the glass vessel was cooled down to room temperature, and 1.0 mL of tetrahydrofuran (THF) was added for the complete recovery and diluting of the substances. The resulting solution was recovered by filtration and analyzed by gas chromatograph using a Shimadzu GC–14B with a flame ionization detector equipped with an InertCap® 1 capillary column.

5.3. Results and discussions

Figure 5.1 shows XRD patterns of UiO-66-X before and after CVD treatment. The XRD pattern of UiO-66-H before CVD treatment was coincident with the previously-reported pattern [11,12]. Moreover, no significant change in the XRD pattern was observed after CVD treatment (Figure 5.1(d), UiO-66-H-$Cr(CO)_3$). It was also found from the N_2 adsorption isotherm that UiO-66-H has a high BET specific surface area of 1031 m^2/g and its specific surface area was nearly unchanged after CVD treatment (958 m^2/g). These results suggest that UiO-66-H possesses a 3-dimentinal porous network structure, and that the post-synthetic CVD treatment does not affect its structure. Figure 5.2 shows the TPD profile of CO elimination from UiO-66-H-$Cr(CO)_3$. The CO elimination peak of UiO-66-H-$Cr(CO)_3$ was observed around 473–533 K. Given that the temperature of decomposition of the molecular chromium hexacarbonyl and benzene chromium tricarbonyl complexes are known to be 423 K and 483 K, respectively [9,16], [–$ArCr(CO)_3$–] complexes are considered to be constructed within the UiO-66-H framework though the CVD treatment (Scheme 5.1). As is the case in UiO-66-H-$Cr(CO)_3$, the framework structures of UiO-66-Br-$Cr(CO)_3$ and UiO-66-NH_2-$Cr(CO)_3$ were maintained even after the construction of [–$ArCr(CO)_3$–] complexes though the CVD treatment (Figure 5.1).

Figure 5.3 shows FT–IR spectra of UiO-66-X before and after CVD treatment. As reference compounds, FT–IR spectra of $Cr(CO)_6$ loaded on MCM-41, which is prepared by a physical vapor deposition method for 40 min in vacuo, and molecular $C_6H_4(COOH)_2Cr(CO)_3$ complex are also shown in Figure 5.3. The molecular $C_6H_4(COOH)_2Cr(CO)_3$ complex exhibited two kinds of IR-active CO vibrational peaks at around 1999 and 1933 cm^{-1} corresponding to $\nu(CO)_{a1}$ and $\nu(CO)_e$ vibrational modes, respectively, while $Cr(CO)_6$ loaded on MCM-41 exhibited mainly one strong IR-active CO vibrational peak at around 1991 cm^{-1} corresponding to $\nu(CO)_{Eg}$ vibrational mode [17,18]. Before CVD treatment, UiO-66-H

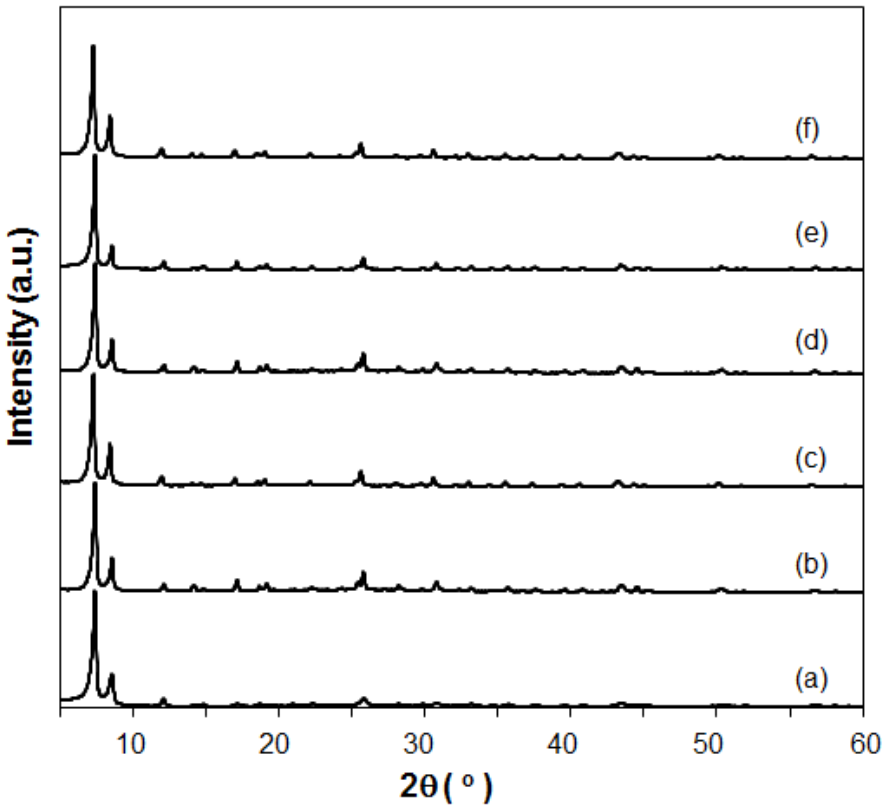

Figure 5.1 XRD patterns of UiO-66-X before and after CVD treatment. (a) UiO-66-Br, (b) UiO-66-H, (c) UiO-66-NH_2, (d) UiO-66-Br-$Cr(CO)_3$, (e) UiO-66-H-$Cr(CO)_3$ and (f) UiO-66-NH_2-$Cr(CO)_3$.

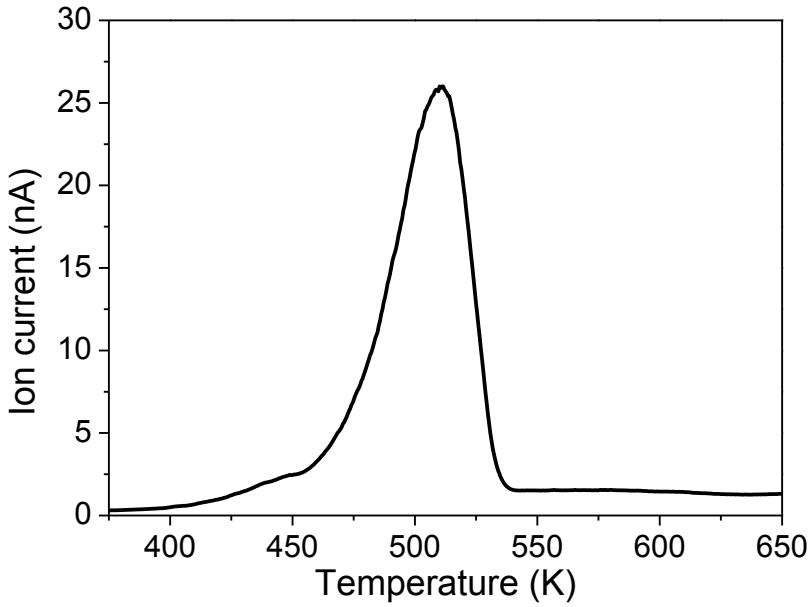

Figure 5.2 TPD profile of CO elimination from UiO-66-H-$Cr(CO)_3$.

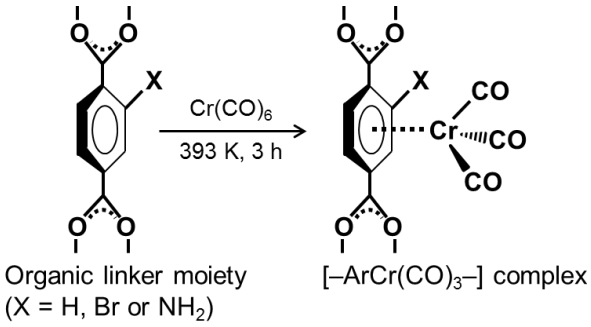

Scheme 5.1

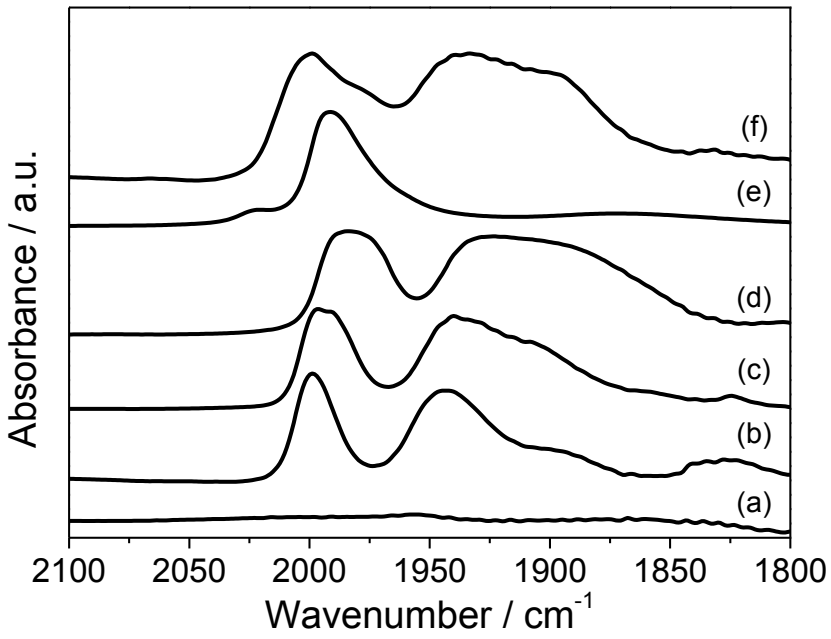

Figure. 5.3 FT–IR spectra of (a) UiO-66-H, (b) UiO-66-Br-$Cr(CO)_3$, (c) UiO-66-H-$Cr(CO)_3$, (d) UiO-66-NH_2-$Cr(CO)_3$, (e) $Cr(CO)_6$ loaded on MCM-41 and (f) $C_6H_4(COOH)_2Cr(CO)_3$.

Table 5.1 IR-active CO vibrational peaks of UiO-66-X-$Cr(CO)_3$.

Sample	Peak position / cm^{-1}	
	$\nu(CO)_{a1}$	$\nu(CO)_e$
UiO-66-Br-$Cr(CO)_3$	1999	1944
UiO-66-H-$Cr(CO)_3$	1997	1940
UiO-66-NH_2-$Cr(CO)_3$	1985	1924
UiO-66-H	–	–

showed no peaks in the measurement range (Figue 5.3(a)). By contrast, obvious peaks were observed at around 1997 cm^{-1} and 1940 cm^{-1} that correspond to $\nu(CO)_{a1}$ and $\nu(CO)_e$ vibrational modes, respectively, in the spectrum of UiO-66-H after CVD treatment (Figue 5.3(c), UiO-66-H-$Cr(CO)_3$). This finding indicates that [–$ArCr(CO)_3$–] complexes are constructed within the UiO-66-H framework though CVD treatment, in which chromium centers are directly coordinated to benzene rings belonging to the organic linker of MOFs. UiO-66-Br and UiO-66-NH_2 also showed similar spectra with two peaks corresponding to $\nu(CO)_{a1}$ and $\nu(CO)_e$ vibrational modes. Thus, the CVD treatment was found to be an effective methodology to form [–$ArCr(CO)_3$–] complexes on arene rings of UiO-66-type MOFs regardless of the type of substituents. On the other hand, the effect of substituents on positions of these peaks was clearly observed. As summarized in Table 5.1, their peak positions were shifted to lower wavenumber in order of decreasing electron withdrawing ability of substituents (UiO-66-Br-$Cr(CO)_3$ > UiO-66-H-$Cr(CO)_3$ > UiO-66-NH_2-$Cr(CO)_3$). Considering that the same substituent effect was reported previously for molecular arenetricarbonyl chromium complexes, chromium centers of the formed [–$ArCr(CO)_3$–] complexes constructed within UiO-66-type MOFs will have closely similar coordination environments [19-21].

In order to assess the catalytic performance of UiO-66-X-$Cr(CO)_3$, the dehydrochlorination of 2-chloro-2-methylbutane was performed in a solid–gas reaction system. In this reaction, arenetricarbonyl chromium complexes act as catalysts to produce 2-methyl-1-butene and 2-methyl-2-butene, accompanied by the formation of HCl (Scheme 5.2). The tridentate arene ligand partially dissociates from the metal center to form a mono- or bidentate ligand, resulting in the creation of coordinatively unsaturated sites which act as catalytically active sites during the reaction [22]. The results of the catalytic tests are summarized in Table 2. All the UiO-66-X-$Cr(CO)_3$ catalysts promoted the

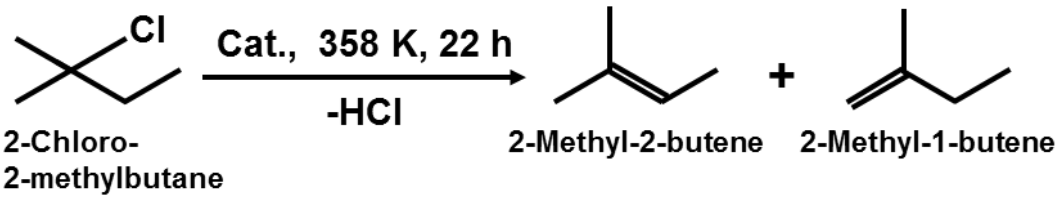

Scheme 5.2

Table 5.2 Dehydrochlorination of 2-chloro-2-methylbutane over various catalysts performed in a solid–gas reaction system at 523 K.

Catalyst	Yields of products / %	
	2-Methyl-2-butene	2-Methyl-1-butene
UiO-66-Br-$Cr(CO)_3$	8.3	0.7
UiO-66-H-$Cr(CO)_3$	9.7	0.6
UiO-66-NH_2-$Cr(CO)_3$	22.4	2.7
UiO-66-H	6.3	0.4

dehydrochlorination reaction and gave 2-methyl-2-butene with high selectivity. Although the progression of the reaction was also observed by using UiO-66-H without [–ArCr(CO)$_3$–] complexes, its catalytic activity was the lowest. This result indicates that [–ArCr(CO)$_3$–] complexes constructed within UiO-66-X act as effective catalysts for the dehydrochlorination of 2-chloro-2-methylbutane. Among those explored, UiO-66-NH$_2$-Cr(CO)$_3$ exhibited the highest catalytic activity, which was much greater than those of UiO-66-H-Cr(CO)$_3$ and UiO-66-Br-Cr(CO)$_3$. Dehydrochlorination reactions are known to be promoted in the presence of base because base accelerates the proton elimination process [23]. In the UiO-66-NH$_2$-Cr(CO)$_3$-catalyzed system, basicity of the –NH$_2$ group substituted to benzene rings of the MOF would play an important role in the enhancement of catalytic activity. Thus, the concerted catalysis in dehydrochlorination of 2-chloro-2-methylbutane was realized via the construction of [–ArCr(CO)$_3$–] complexes and the functionalization of MOFs by introducing substituent groups. Since this method enables us to confine catalytically active sites near surface functional sites, it will open new opportunities for the development of unique and effective heterogeneous catalysts.

5.4. Conclusions

In summary, [–ArCr(CO)$_3$–] complexes were successfully constructed within UiO-66-type Zr-based MOFs with different substituent groups (UiO-66-X; X = Br, H or NH$_2$) by a CVD treatment using Cr(CO)$_6$ as a starting material. Characterization studies revealed that the chromium centers of the complexes were directly coordinated to arene rings belonging to organic linkers of the MOFs, regardless of the type of substituent groups. Moreover, a substituent effect similar to molecular arenetricarbonyl chromium complexes was observed in FT–IR spectra of the constructed [–ArCr(CO)$_3$–] complexes, in which peak positions assignable to CO vibrational modes were shifted to lower wavenumber in order of decreasing

electron withdrawing ability of substituents. [–ArCr(CO)$_3$–] complexes constructed within UiO-66-X (UiO-66-X-Cr(CO)$_3$) exhibited an efficient catalytic activity for dehydrochlorination of 2-chloro-2-methylbutane to produce 2-methyl-2-butene with high selectivity. It is noteworthy that UiO-66-NH$_2$-Cr(CO)$_3$ showed the highest catalytic activity due to a concerted effect between basicity of –NH$_2$ groups and catalysis of [–ArCr(CO)$_3$–] complexes.

5.5. References

[1] K. Schlichte, T. Kratzke, S. Kaskel, Micropor. Mesopor. Mater., **73**, 81 (2004).

[2] R. Banerjee, A. Phan, B. Wang, C. Knobler, H. Furukawa, M. O_Keeffe, O. M. Yaghi, Science, **319**, 939 (2008).

[3] S. Kitagawa, R. Kitaura, S. Noro, Angew. Chem., Int. Ed., **43**, 2334 (2004).

[4] M. Dinca, J. R. Long, J. Am. Chem. Soc., **127**, 9376 (2005).

[5] H. Bux, F. Liang, Y. Li, J. Cravillon, M. Wiebcke, J. Caro, J. Am. Chem. Soc., **131**, 16000 (2009).

[6] F. Vermoortele, R. Ameloot, A. Vimont, C. Serrec, D.D. Vos Chem. Commun., **47**, 1521 (2011).

[7] G. Akiyama, R. Matsuda, H. Sato, M. Takata, S. Kitagawa, Adv. Mater., **23**, 3294 (2011).

[8] S.S. Kaye, J. R. Long, J. Am. Chem. Soc., **130**, 806 (2008).

[9] S. Chavan, J.G. Vitillo, M.J. Uddin, F. Bonino, C. Lamberti, E. Groppo, K.-P. Lillerud, S. Bordiga, Chem. Mater., **22**, 4602 (2010).

[10] C. Wang, Z. Xie, K.E deKrafft, W. Lin, J. Am. Chem. Soc., **133**, 13445 (2011).

[11] J.H. Cavka, S. Jakobsen, U. Olsbye, N. Guillou, C. Lamberti, S. Bordiga, K.P. Lillerud, J. Am. Chem. Soc., **130**, 13850 (2008).

[12] M. Kandiah, M. H. Nilsen, S. Usseglio, S. Jakobsen, U. Olsbye, M. Tilset, C. Larabi, E. A. Quadrelli, F. Bonino, K. P. Lillerud, Chem. Mater., **22**, 6632 (2010).

[13] T. Kamegawa, T. Sakai, M. Matsuoka, M. Anpo, J. Am. Chem. Soc., **127**, 16784 (2005).

[14] M. Matsuoka, T. Kamegawa, T. H. Kim, T. Sakai, M. Anpo, J. Nanosci. Nanotechnol., **10**, 314 (2010).

[15] T. Kamegawa, M. Saito, T. Sakai, M. Matsuoka, M. Anpo, Catal. Today, **181**, 14 (2012).

[16] E. Patsalides, S.J. Pratten, J. Organomet. Chem., **364**, 169 (1989).

[17] Y. Huang, R.R. Poissant, Langmuir, **18**, 5487 (2002).

[18] G. Hunter, C.H. Rochester, A.G. Wilkinson, J. Paton, J. Chem. Soc. Faraday Trans., **92**, 5093 (1996).

[19] Neuse E. W.: J. Organomet. Chem., **99**, 287 (1975).

[20] A.D. Hunter, L.Shilliday, Organometallics, **11**, 1550 (1992).

[21] A.D. Hunter, V. Mozol, S.D. Tsai, Organometallics, **11**, 2251 (1992).

[22] Unsaturated site T.P.Tsonis, J.S. Hwang, J. Mol. Catal., **26**, 219 (1984).

[23] I. Mochida, A. Uchino, H. Fujitsu, K. Takeshita, J. Catal., **43**, 264 (1976).

Chapter 6

Effect of Pore Size on Catalytic Activities of Arenetricarbonyl Complexes ([–$C_6H_4M(CO)_3$–]; M = Mo, Cr) Constructed within Zr-Based MOFs

6.1. Introduction

There has been intensive interest in the immobilization of guest molecules onto solid surfaces in the light of the unique and efficient material design enabling the integration of controlled chemical properties at molecular level and the rigidity of solid supports. Heretofore, various combinations of guest molecules and solid supports have been attempted for applications to catalysts, luminescence materials, sensors and so on [1-6]. Among those, in the field of catalysts, organometallic complex molecules occupy the interest of researchers, because they often exhibit excellent catalytic reactivity with high activity and selectivity, and their catalytic reactivity readily tuned by varying their ligands [7-8]. In addition, the immobilization of organometallic complex molecules onto solid supports enables the transformation of processes from homogeneous to heterogeneous. The utilization of the heterogeneous catalytic system will be able to reuse the catalysts and to reduce time consuming and extra purification processes caused by use of homogeneous catalysts.

On the other hand, since characteristics of organometallic complexes as guest molecules are influenced strongly by steric and electrostatic constraints derived from solid supports, the design of an appropriate reaction field by the selection of solid supports is of significant important [9,10]. Metal–organic framework (MOFs) also called as porous coordination polymers (PCPs) are promising candidate materials for solid supports owing to their extremely high specific surface areas and large pore volumes [11,12]. In addition to these unique features, the structures and chemical properties of MOFs can be varied by changing the assemblage of organic linkers and metal nodes constituting their microporous frameworks. So far, for example, unique adsorbents and acid or base catalysts have been developed by using organic linkers bearing various substituent groups [2,11-14]. Moreover, Kaye et al. have reported the construction of organochromium complexes within frameworks of MOFs by using a ligand exchange reaction between chromium hexacarbonyl ($Cr(CO)_6$) and benzene

rings belonging to organic linkers of MOFs [15,16]. In these complexes, chromium centers are directly coordinated to benzene rings within frameworks of MOFs. Such organometallic complexes constructed within MOF frameworks are expected to exhibit high catalytic performances owing to their closely similar coordination environments to molecular ones. Accurate design of reaction fields taking advantage of the structure diversity of MOFs makes it possible to develop unique and efficient heterogeneous organometallic complexes catalysts.

In the present study, arenetricarbonyl complexes ([–$C_6H_4M(CO)_3$–]; M = Mo, Cr) have been constructed within Zr-based MOFs with different pore sizes (UiO-66 and UiO-67), and their heterogeneous catalytic activities have been evaluated. The detailed characterization of local structures of [–$C_6H_4M(CO)_3$–] complexes and effects of pore size on their catalytic activities are described and discussed below.

6.2. Experimental

Synthesis of Zr-based MOFs

Zr-based MOFs named UiO-66 and UiO-67 was prepared by a conventional solvothermal method using 1,4-benzenedicarboxylic acid (BDC) and 4,4'-biphenyldicarboxylic acid (BPDC) as organic linkers, respectively [17]. The typical synthesis procedure for UiO-66 was as follows. BDC (1.64 mmol) and zirconium tetrachloride ($ZrCl_4$, 1.80 mmol) were dissolved in N,N-dimethylformamide (DMF, 211 mL) and stirred for few minutes at room temperature. The mixture was then placed in a Teflon-lined stainless-steel autoclave and heated in oven at 393 K for 24 h. After cooling to room temperature, the precipitate was filtered, washed repeatedly with DMF and dried at room temperature for 24 h. The obtained white powder sample was then dried under vacuum at 473 K for 2 h to remove residual DMF, yielding UiO-66. UiO-67 was prepared by a similar procedure using BPDC as an organic linker. The precursor solution prepared by mixing BPDC (1.36 mmol), $ZrCl_4$ (1.36 mmol)

and DMF (158 mL) was stirred for 30 min at room temperature, placed in a Teflon-lined stainless-steel autoclave and heated in oven at 393 K for 48 h. After cooling to room temperature, the precipitate was filtered, washed repeatedly with DMF and dried at room temperature for 24 h. The obtained white powder sample was then dried under vacuum at 473 K for 2 h to remove residual DMF.

Construction of [–$C_6H_4M(CO)_3$–] complexes within UiO-66 and UiO-67

[–$C_6H_4M(CO)_3$–] complexes were constructed within UiO-66 and UiO-67 by a chemical vapor deposition (CVD) technique [18,19,20]. Specifically, in the synthesis of [–$C_6H_4Mo(CO)_3$–] complexes, UiO-66 or UiO-67 degassed at 473 K for 1 h to remove the adsorbed water molecules on the surface was subject to $Mo(CO)_6$ vapor at 373 K for 3 h in vacuo. After that, unreacted and physisorbed $Mo(CO)_6$ was removed by evacuation at 423 K for 1 h, yielding UiO-66-$Mo(CO)_3$ or UiO-67-$Mo(CO)_3$. The [–$C_6H_4Cr(CO)_3$–] complexes constructed within UiO-66 and UiO-67 (UiO-66-$Cr(CO)_3$ and UiO-67-$Cr(CO)_3$, respectively) were prepared by the same method except the CVD treatment was performed at 393 K using $Cr(CO)_6$ as a starting material.

Characterization of [–$C_6H_4M(CO)_3$–] complexes within UiO-66 and UiO-67

XRD (X-ray diffraction) data were recorded on a Shimadzu XRD-6100 using Cu Kα radiation (λ = 1.5406 Å). FT–IR (Fourier-transform infrared spectroscopy) data were recorded with a Jasco FT/IR-660 plus.

Selective oxidation reaction

The epoxidation of cyclooctene was carried out in a closed glass reaction vessel (20 mL) at 328 K under N_2 atmosphere. The reaction vessel was loaded with 30 mg of catalyst, 1.7

mmol of cyclooctene and 2.7 mmol of tert-butyl hydroperoxide (TBHP, 5.5 M in decane). In order to avoid the photodissociation of the carbonyl ligands caused by interaction with reagents or solvent [21,22], the catalytic tests were carried out in the dark. After the reaction (15 min or 3 h), the reaction mixture was cooled down to 298 K and then filtered to remove the catalyst. Analysis of the products was performed on a gas chromatograph (Shimadzu GC–14B with a flame ionization detector) equipped with an InertCap®1 capillary column.

6.3. Results and discussions

Figure 6.1 and 6.2 show XRD patterns of UiO-66 and UiO-67 before and after CVD treatments for the construction of [–$C_6H_4M(CO)_3$–] complexes, respectively. The diffraction patterns of UiO-66 and UiO-67 before CVD treatment were in good agreement with previously-reported patterns, indicating the successful formation of MOF framework structures having micropores [17,23,24]. It should be noted that the position of the diffraction peak at the lowest angle in the pattern of UiO-67 ($2\theta = 6°$), which is associated with the pore size, was lower than that of UiO-66 ($2\theta = 8°$). This finding represents that the longer organic linker, BPDC, leads to the expansion of the pore size of UiO-67 as compared to UiO-66. After CVD treatment, the diffraction patterns of UiO-66 and UiO-67 were nearly unchanged regardless of the kinds of starting materials (*i.e.*, $Cr(CO_6)$ or $Mo(CO)_6$), suggesting that the CVD treatment for the immobilization of metal complexes onto UiO-66 and UiO-67 did not influence their framework structures.

Subsequently, FT–IR measurements were performed to confirm the formation of arenetricarbonyl complexes within MOF frameworks. FT–IR spectra were collected after evacuation at 473 K or 523 K for 1 h. Figure 6.3 shows FT–IR spectra of UiO-66-$Mo(CO)_3$ and UiO-67-$Mo(CO)_3$ evacuated at 473 K and 523 K. UiO-66 and UiO-67 before CVD

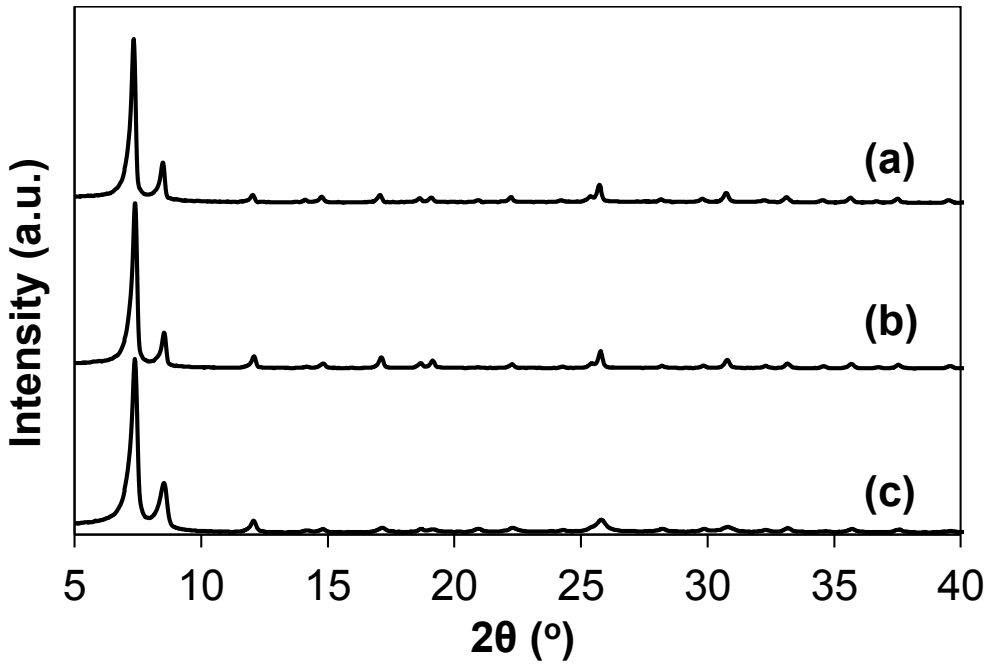

Figure 6.1 XRD patterns of (a) UiO-66-$Mo(CO)_3$, (b) UiO-66-$Cr(CO)_3$ and (c) UiO-66.

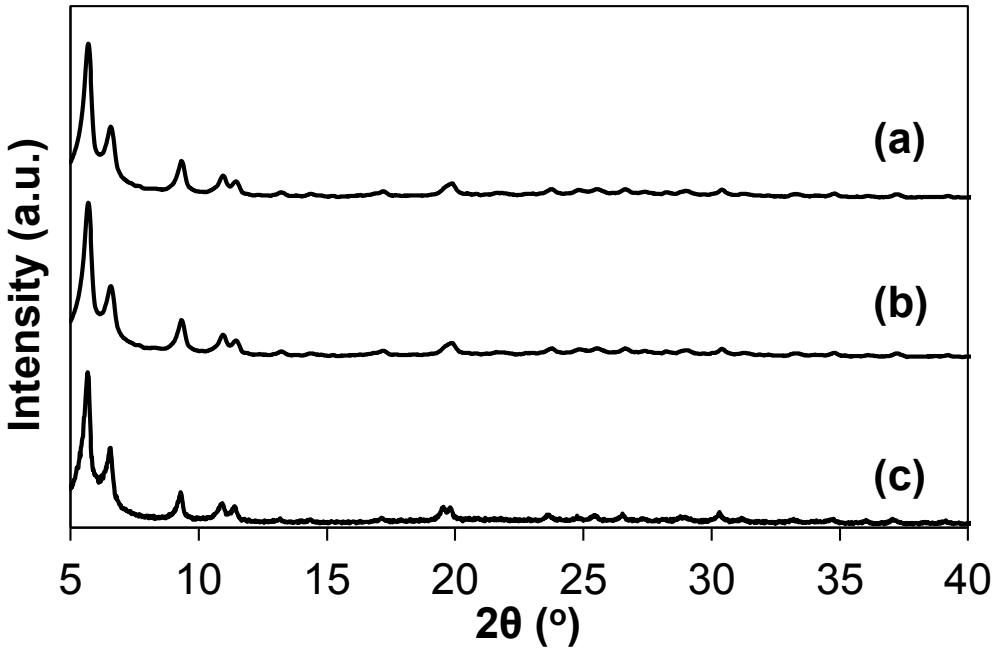

Figure 6.2 XRD patterns of (a) UiO-67-$Mo(CO)_3$, (b) UiO-67-$Cr(CO)_3$ and (c) UiO-67.

treatments exhibited no peaks in the measurement range (data not shown). After CVD treatments, observable peaks were seen in spectra of UiO-66-$Mo(CO)_3$ and UiO-67-$Mo(CO)_3$ evacuated at 473 K around 1990–1980 cm^{-1} and 1940–1910 cm^{-1}. In general, the molecular $C_6H_6Mo(CO)_3$ complex shows two kinds of IR-active CO vibrational peaks at 1987 and 1916 cm^{-1} assignable to $\nu(CO)_{a1}$ and $\nu(CO)_e$ vibrational modes, respectively [25]. By contrast, the IR spectrum of $Mo(CO)_6$ has mainly one strong IR-active CO vibrational peak at 1985 cm^{-1} assignable to $\nu(CO)_{Eg}$ vibrational mode [25]. These results and information suggest that molybdenum center is directly coordinated to phenylene and biphenylene rings belonging to organic linkers of MOFs though the CVD treatment to form [$–C_6H_4Mo(CO)_3–$] complexes within MOFs (Scheme 6.1). Furthermore, these CO vibrational peaks of [$–C_6H_4Mo(CO)_3–$] complexes constructed within UiO-67 were shifted to lower wavenumbers than those within UiO-66. These peak shifts were attributed to high electron-donating power of biphenylene moieties of UiO-67 [26]. These CO vibrational peaks completely disappeared after evacuation at 523 K for 1 h. This finding indicates that the arenetricarbonyl complexes were decomposed by heat treatments. Similar results were obtained in FT–IR spectra of UiO-66-$Cr(CO)_3$ and UiO-67-$Cr(CO)_3$ (Figure 6.4). Thus, the [$–C_6H_4Cr(CO)_3–$] complexes were also constructed within UiO-66 and UiO-67.

Molybdenum tricarbonyl complexes are known to be one of the effective catalysts for epoxidation of olefins with tert-butyl hydroperoxide (TBHP) as an oxidant. In these reactions, molybdenum tricarbonyl complexes undergo oxidative decarbonylation with TBHP to form oxomolybdenum(VI) species, such as Cp'MoO_2X and/or Cp'$MoO(O_2)X$ [1,21,22]. These oxomolybdenum(VI) species act as highly active catalytic sites for the epoxidation reaction with TBHP as an oxidant. Based on the successful formation of arenetricarbonyl complexes within MOFs, epoxidation of cyclooctene with TBHP over UiO-66-$Mo(CO)_3$ and UiO-67-$Mo(CO)_3$ was attempted under N_2 atmosphere (Scheme 6.2). UiO-66-$Cr(CO)_3$ and

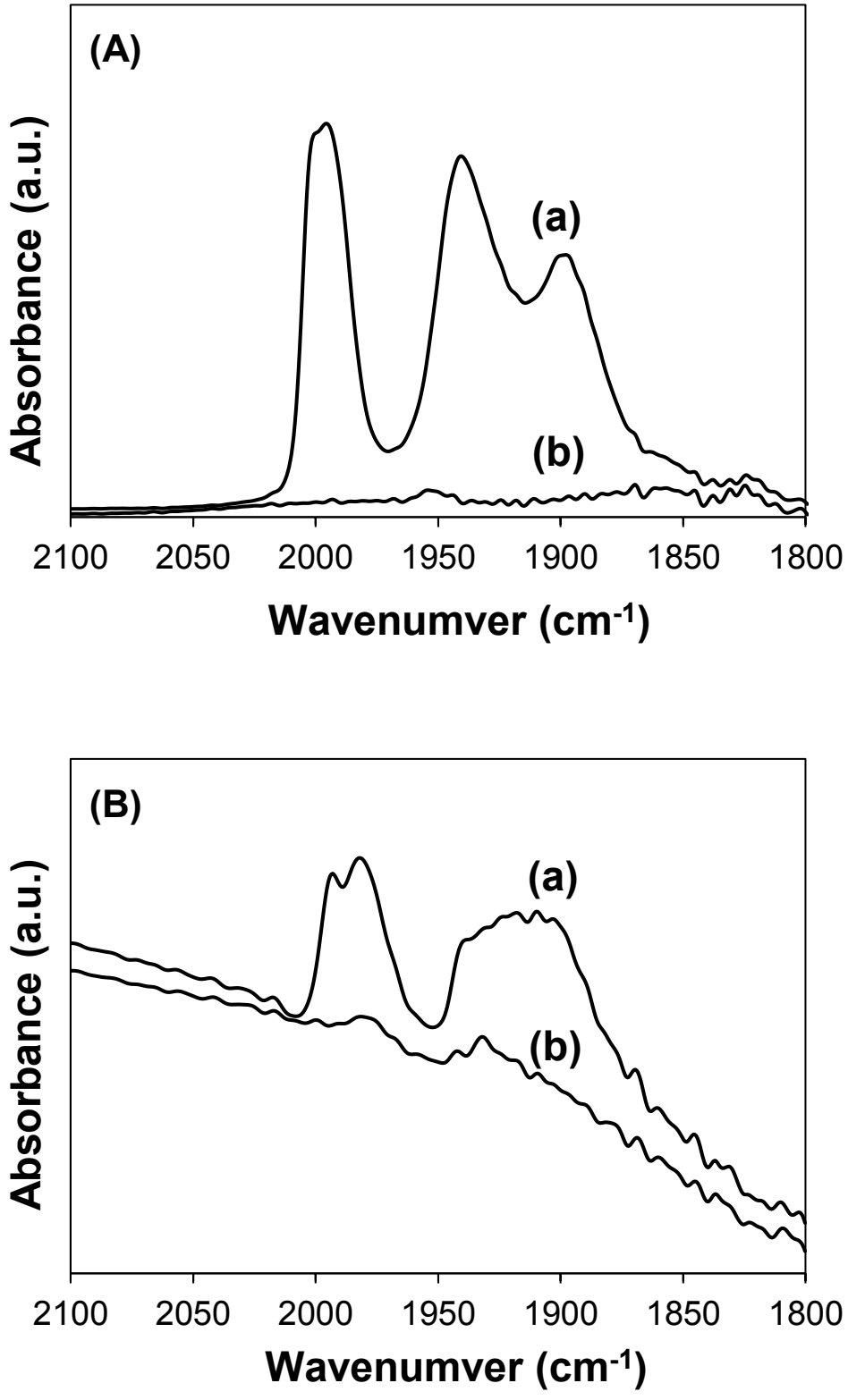

Figure 6.3 FT–IR spectra of (A) UiO-66-$Mo(CO)_3$ and (B) UiO-67-$Mo(CO)_3$ after evacuation at (a) 473 K and (b) 523 K for 1 h.

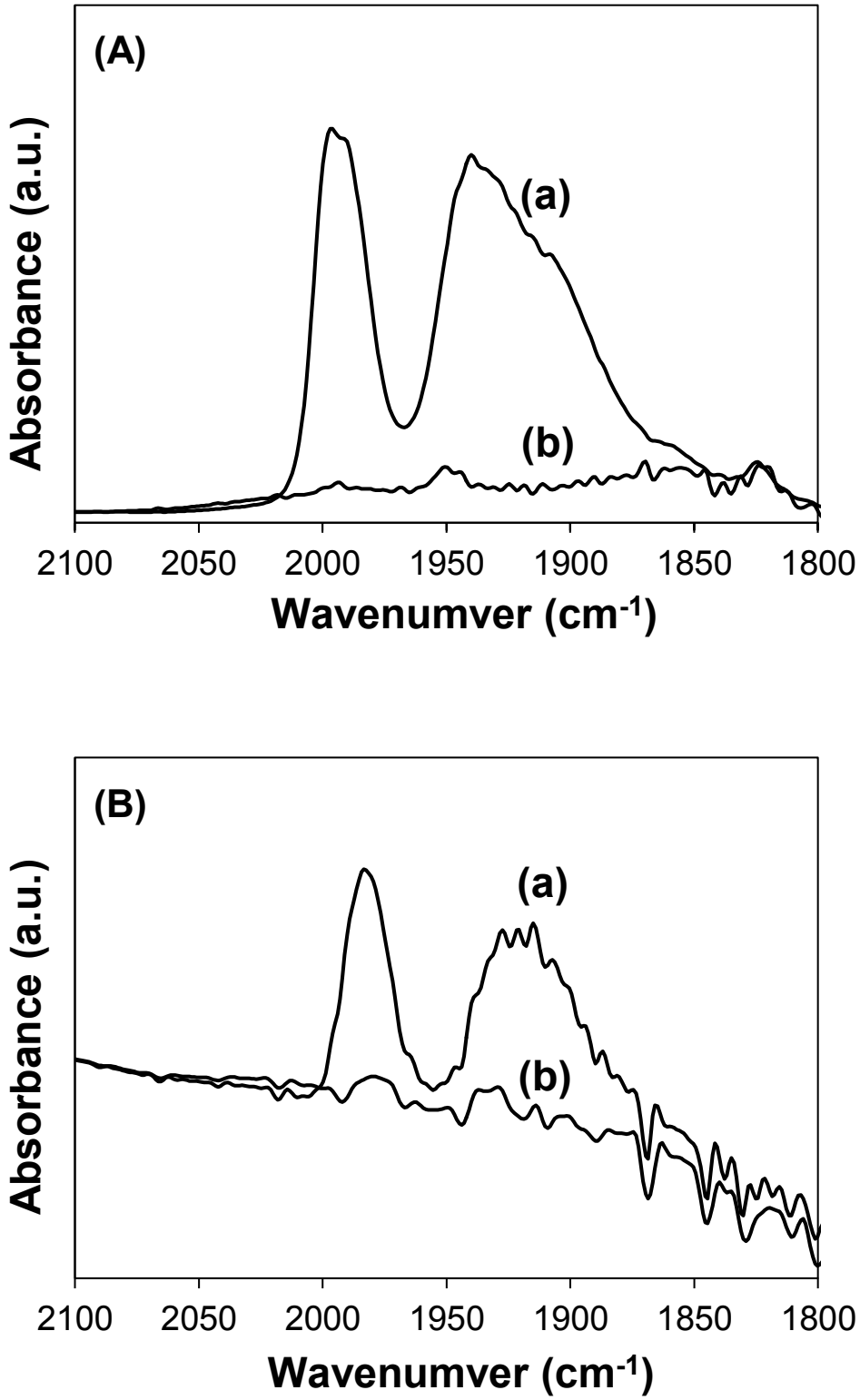

Figure 6.4 FT–IR spectra of (A) UiO-66-$Cr(CO)_3$ and (B) UiO-67-$Cr(CO)_3$ after evacuation at (a) 473 K and (b) 523 K for 1 h.

UiO-67-Cr(CO)$_3$ were also employed as catalysts. As shown in Table 6.1, UiO-66-Mo(CO)$_3$ and UiO-67-Mo(CO)$_3$ promoted the epoxidation reaction and gave cyclooctene oxide with almost 100% selectivity. In contrast, the epoxidation reaction hardly proceeded over UiO-66 and UiO-67 without [–C_6H_4M(CO)$_3$–] complexes. These results indicate that arenetricarbonyl complexes constructed within MOFs act as effective catalytically active sites. Although UiO-66-Cr(CO)$_3$ and UiO-67-Cr(CO)$_3$ showed catalytic activities for the epoxidation reaction, their catalytic activities were lower than that of UiO-66-Mo(CO)$_3$ and UiO-67-Mo(CO)$_3$. It is noteworthy that UiO-67-M(CO)$_3$ showed higher activity than UiO-66-M(CO)$_3$. These catalytic enhancements would be due to the difference in the facility of substance diffusion between UiO-67 and UiO-66. Although both porous structures consist of an array of tetrahedral and octahedral cavities, the longer organic linker, BPDC, leads to the expansion of pores of UiO-67 compared with UiO-66. The diameters of tetrahedral and octahedral micropores in UiO-67 (12 and 16 Å, respectively) are larger than those in UiO-66 (7.5 and 12 Å, respectively) [24]. Since the tetrahedral pore size of UiO-66 (7.5 Å) is smaller than the molecular size of cyclooctene (ca. 8 Å), substance diffusion is considered to influence their catalytic activities strongly. These data indicate that the accessibility of cyclooctene to catalytically active [–C_6H_4M(CO)$_3$–] complexes is partially-hindered by smaller pores in UiO-66. Hence, the catalytic activity of UiO-67-Mo(CO)$_3$ was higher than UiO-66-Mo(CO)$_3$. In these reactions, oxomolybdenum (VI) species formed during the reaction would be promoted the epoxidation of cyclooctene as follows; the formed complexes coordinate with TBHP at molybdenum center and react with cyclooctene to produce cyclooctene oxide and tert-BuOH as a by-product [27,28]. In fact, the amount of tert-BuOH equivalent to that of the cyclooctene oxide was obtained. This result provides evidence to support the reaction mechanism.

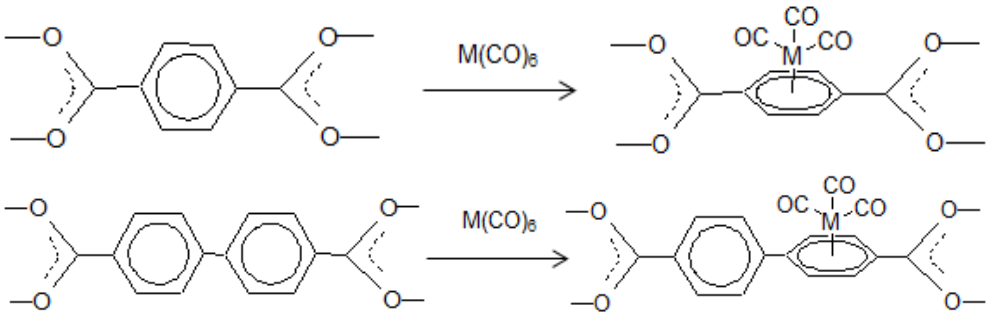

Scheme 6.1

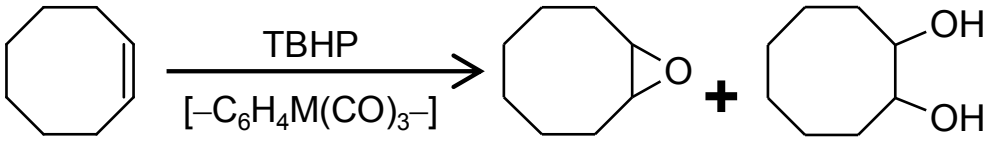

Scheme 6.2

Table 6.1 Epoxidation of cyclooctene with TBHP on various catalysts at 328 K.

Catalyst	Reaction time (min)	Conv. (%)	Sel. (%)[a]
No catalyst	15	trace	-
UiO-66(H)	15	trace	-
UiO-66(H)-$Mo(CO)_3$	15	68	>99
UiO-66(NH_2)-$Mo(CO)_3$	15	63	>99
UiO-66(Br)-$Mo(CO)_3$	15	60	>99
UiO-67-$Mo(CO)_3$	15	92	>99
UiO-66-$Cr(CO)_3$	180	29	>99
UiO-67-$Cr(CO)_3$	180	43	>99
UiO-67-$Mo(CO)_3$	180	100	>99
UiO-67-$Mo(CO)_3$ 2nd run	180	100	>99
UiO-67-$Mo(CO)_3$ 3rd run	180	97	>99

[a] Selectivity to cyclooctene oxide.

On the other hand, epoxide groups are known to react with water and alcohol into diol and ether, respectively, in the presence of Lewis acid [29]. Considering the fact that Zr clusters within UiO-67 act as Lewis acid catalysts and that reaction mixture contains water derived from commercially available TBHP and tert-BuOH as the by-product, the produced epoxide seems to react with them when the reaction time is prolonged [6]. In order to investigate the influence of reaction time on epoxide selectivity, the epoxidation reaction was carried out over UiO-67-$Mo(CO)_3$ upon prolonged reaction time (from 15 min to 180 min). The conversion of cyclooctene reached almost 100% after 3 h. It should be noted that the selectivity of cyclooctene oxide remained nearly unchanged, even prolong the reaction time. This result reveals that Zr clusters within UiO-67-$Mo(CO)_3$ did not act as Lewis acid under this reaction conditions, resulting that UiO-67-$Mo(CO)_3$ showed excellent selectivity. Finally, the reusability of UiO-67-$Mo(CO)_3$ was investigated. After the reaction, the solid catalyst was collected by filtration, washed several times with n-hexane, dried at room temperature and reused in next catalytic cycle. The recovered catalyst was found to be recycled without significant loss of its catalytic activity at least 2 times, suggesting that the [–$C_6H_4Mo(CO)_3$–] complex is stably present in UiO-67 and acts as a reusable heterogeneous catalyst.

6.4. Conclusions

In summary, the [–$C_6H_4M(CO)_3$–] complexes were successfully constructed within UiO-66 and UiO-67 by a CVD treatment using $M(CO)_6$ as a starting material. The metal centers of the complexes were directly coordinated to arene rings belonging to organic linkers of the MOFs regardless of the kinds of starting materials as well as the different pore size of MOFs. Moreover, the MOF framework structures were found to be maintained even after the construction of [–$C_6H_4M(CO)_3$–] complexes through the CVD treatment. FT–IR

measurements revealed that the constructed [–$C_6H_4M(CO)_3$–] complexes were decomposed by heat treatment at 523 K for 1 h. The [–$C_6H_4M(CO)_3$–] complexes constructed within UiO-66 and UiO-67 (UiO-66-$M(CO)_3$ and UiO-67-$M(CO)_3$) exhibited high catalytic activities and selectivities for epoxidation of cyclooctene with TBHP. Moreover, [–$C_6H_4Mo(CO)_3$–] complexes showed higher catalytic activity than [–$C_6H_4Cr(CO)_3$–] complexes. It is noteworthy that UiO-67-$M(CO)_3$ showed higher activity than UiO-66-$M(CO)_3$, which indicated that the accessibility of substrates to catalytically active [–$C_6H_4M(CO)_3$–] complexes was partially-hindered by smaller pores in UiO-66. Furthermore, the selectivity of cyclooctene oxide remained nearly unchanged, even prolong the reaction time. The recovered UiO-67-$M(CO)_3$ showed higher activity than UiO-66-$M(CO)_3$ catalyst was found to be recycled without significant loss of its catalytic activity at least 2 times, suggesting that the [–$C_6H_4Mo(CO)_3$–] complex is stably present in UiO-67 and acts as a reusable heterogeneous catalyst.

6.5. References

[1] C. Freund, M. Abrantes, F.E. Kühn, J. Organomet. Chem., **691**, 3718 (2006).

[2] F. Vermoortele, R. Ameloot, A. Vimont, C. Serrec, D.D. Vos, Chem. Commun., **47**, 1521 (2011).

[3] L-N. Sun, H-J. Zhang, C-Y Peng, J-B. Yu, Q-G. Meng, L-S. Fu, F-Y. Liu, X-M. Guo, J. Phys. Chem. B, **110**, 7249 (2006).

[4] K. Mori, M. Tottori, K. Watanabe, M. Che, H. Yamashita, J. Phys. Chem. C, **115**, 21358 (2011).

[5] K. Mori, K. Watanabe, Y. Terai, Y. Fujiwara, H. Yamashita, Chem. Eur. J., **18**, 11371 (2012).

[6] H. Zhang, Y. Sun, K. Ye, P. Zhang, Y. Wang, J. Mater. Chem., **15**, 3181 (2005).

[7] E.L. Grognec, J. Claverie, R. Poli, J. Am. Chem. Soc., **123**, 9513 (2001).

[8] A. Gu¨ nyar, D. Betz, M. Drees, E. Herdtweck, F.E. Ku¨hn, J. Mol. Catal. A: Chem., **331**, 117 (2010).

[9] S. Inagaki, O. Ohtani, Y. Goto, K. Okamoto, M. Ikai, K. Yamanaka, T. Tani, T. Okada, Angew. Chem. Int. Ed., **48**, 4042 (2009).

[10] T. Kamegawa, M. Saito, T. Watanabe, K. Uchihara, M. Kondo, M. Matsuoka, M. Anpo, J. Mater. Chem., **21**, 12228 (2011).

[11] R. Banerjee, A. Phan, B. Wang, C. Knobler, H. Furukawa, M. O'Keeffe, O.M. Yaghi, Science, **319**, 939 (2008).

[12] S. Kitagawa, R. Kitaura, S. Noro, Angew. Chem. Int. Ed., **43**, 2334 (2004).

[13] C.A. Bauer, T.V. Timofeeva, T.B. Settersten, B.D. Patterson, V.H. Liu, B.A. Simmons, M.D. Allendorf, J. Am. Chem. Soc., **129**, 7136 (2007).

[14] G. Akiyama, R. Matsuda, H. Sato, M. Takata, S. Kitagawa, Adv. Mater., **23**, 3294 (2011).

[15] S.S. Kaye, J.R. Long, J. Am. Chem. Soc., **130**, 806 (2008).

[16] S. Chavan, J.G. Vitillo, M.J. Uddin, F. Bonino, C. Lamberti, E. Groppo, K.P. Lillerud, S. Bordiga, Chem. Mater., **22**, 4602 (2010).

[17] J.H. Cavka, S. Jakobsen, U. Olsbye, N. Guillou, C. Lamberti, S. Bordiga, K.P. Lillerud, J. Am. Chem. Soc., **130**, 13850 (2008).

[18] T. Kamegawa, T. Sakai, M. Matsuoka, M. Anpo, J. Am. Chem. Soc., **127**, 16784 (2005).

[19] M. Matsuoka, T. Kamegawa, T-H. Kim, T. Sakai, M. Anpo, J. Nanosci. Nanotechnol., **10**, 314 (2010).

[20] T. Kamegawa, M. Saito, T. Sakai, M. Matsuoka, M. Anpo, Catal. Today, **181**, 14 (2012).

[21] A.C. Coelho, S.S. Balula, S.M. Bruno, J.C. Alonso, N. Bion, P. Ferreira, M. Pillinger, A.A. Valente, J. Rocha, I.S. Goncalves, Adv. Synth. Catal., **352**, 1759 (2010).

[22] A.C. Coelho, S.S. Balula, M.M. Antunes, T.I. Gerganova, N. Bion, P. Ferreira, M. Pillinger, A.A. Valente, J. Rocha, I.S. Goncalves, J. Mol. Catal. A: Chem., **332**, 13 (2010).

[23] A. Schaate, P. Roy, A. Godt, J. Lippke, F. Waltz, M. Wiebcke and P. Behrens, Chem. Eur. J., **17**, 6643 (2011).

[24] S. Chavan, J.G. Vitillo, D. Gianolio, O. Zavorotynska, B. Civalleri, S. Jakobsen, M.H. Nilsen, L. Valenzano, C. Lamberti, K.P. Lillerud, S. Bordiga, Phys. Chem. Chem. Phys., **14**, 1614 (2012).

[25] C.J. Breheny, J.M. Kelly, C. Long, S. O'Keeffe, M.T. Pryce, G. Russell, M.M. Walsh, Organometallics, **17**, 3690 (1998).

[26] S. Antonini, F. Calderazzo, U. Englert. E. Grigiotti, G. Pamaloni, P. Zanello, J. Organomet. Chem., **689**, 2158 (2004).

[27] A.M. Al-Ajlouni, D. Veljanovski, A. Capapé, J. Zhao, E. Herdtweck, M.J. Calhorda, F.E. Kühn, Organometallics, **28**, 639 (2009).

[28] P.J. Costa, M.J. Calhorda, F.E. Kühn, Organometallics, **29**, 303 (2010).

[29] M. Mrak, N.N. Tusar, N.Z. Logar, G. Mali, A. Kljajic, I. Arcon, F. Launay, A. Gedeon, V. Kaucic, Micropor. Mesopor. Mater., **95**, 76 (2006).

Chapter 7

General Conclusions

General Conclusions

In this thesis, the study on the development of single-site heterogeneous catalysts constructed within frameworks of zeolite, MCM-41, HMMs and MOFs by post-synthesis, ligand exchange reaction and CVD methods has been performed. The metal ions, metal complexes and organometallic complexes incorporated into the porous materials were revealed to be present in highly dispersed and isolated states by UV–Vis, photoluminescence, FT–IR, TPD, XAFS, XRD and N_2 adsorption isotherm measurements. Moreover, these single-site species acted as photocatalytic and catalytic sites for various selective heterogeneous reactions, such as photocalytic oxidation of CO with N_2O and decomposition of 2-propanol in water, Mukaiyama aldol reaction of benzaldehyde with 1-trimethylsiloxy cyclohexene, selective hydrosilylation reaction of 1-hexyne with triethylsilane, dehydrochlorination of 2-chloro-2-methylbutane and epoxidation of cyclooctene with TBHP. The main results obtained are summarized below.

Summary of Chapter 2

Chapter 2 deals with characterizations of local structures of active sites in Ti–containing BEA zeolites (TiSiBEA) as well as their photocatalytic activities for the oxidation of CO with N_2O and decomposition of 2-propanol in water. Photoluminescence investigations revealed that the incorporated Ti^{4+} ions within TiSiBEA were present in isolated tetrahedrally coordinated states at low Ti contents, and aggregated species were formed with increase in Ti contents. Photocatalytic studies of TiSiBEA provided evidence that isolated tetrahedral Ti-species play an important role as active site in photocatalytic reactions compared with the octahedral Ti-species since the TiSiBEA containing 3.2 wt.% of Ti exhibited almost same photocatalytic activities as that of TiSiBEA containing 5.8 wt.% of Ti.

Summary of Chapter 3

In Chapter 3, the preparation and characterizations of tin and tin triflate species incorporated within MCM-41 (Sn-MCM-41 and SnOTf-MCM-41, respectively) as well as the catalytic properties for Mukaiyama–aldol reaction of benzaldehyde with 1-trimethylsiloxy cyclohexene at room temperature as Lewis acid catalysts. XRD and UV–Vis measurements revealed that SnOTf-MCM-41 possess highly ordered mesoporous structures and tetrahedrally-coordinated Sn species. In addition, FT–IR analysis identified that triflate ligands are selectively coordinated with Sn^{4+} species in mesoporous silica frameworks. The catalytic studies revealed that Sn-MCM-41 promoted the Mukaiyama-aldol reaction of benzaldehyde with 1-trimethylsiloxy cyclohexene at room temperature as Lewis acid catalysts and gave the syn-products with high selectivity. Moreover, SnOTf-MCM-41 exhibited higher catalytic activities than Sn-MCM-41 with maintaining their high syn-selectivity. Taking into account the results of *in-situ* FT–IR experiments using pyridine as a probe molecule, the enhanced catalytic performance after triflic acid treatment was found to be attributed to the increase in the number of acid sites due to water tolerance of metal triflate species. Furthermore, the SnOTf-MCM-41 catalyst can be reused for the Mukaiyama-aldol reaction at least 3 times.

Summary of Chapter 4

Chapter 4 reported the construction of organoruthenium complexes (–[biphRuCp]PF_6–) within biphenylene–bridged inorganic–organic HMM (HMM–biph) and their catalytic activities for selective hydrosilylation of 1-hexyne with triethylsilane in a solid–gas heterogeneous system. UV–Vis and XAFS studies provided evidence that the structure of the –[biphRuCp]PF_6– complex was closely similar to that of [C_6H_6RuCp]PF_6, suggesting that the biphenylene moiety within HMM–biph directly coordinates to the metal center of the

organoruthenium complex by ligand exchange reaction of HMM–biph with $[(CH_3CN)_3RuCp]PF_6$. The selective hydrosilylation of 1-hexyne was found to proceed efficiently on –[biphRuCp]PF_6– complex constructed within HMM–biph (HMM–biphRuCp) and give α-vinylsilane as a main product. Moreover, HMM–biphRuCp exhibited higher catalytic activity than –[phRuCp]PF_6– complex-constructed within phenylene–bridged HMM (HMM–biphRuCp). This higher catalytic performance of HMM–biphRuCp than HMM–phRuCp can be ascribed to the higher loading amount of the Ru complex into HMM–biph than that into HMM–ph, which is derived from the electron donating ability of biphenylene moieties.

Summary of Chapter 5

Chapter 5 discussed the chemical property of arenetricarbonyl chromium complexes ([–$ArCr(CO)_3$–]) constructed within Zr-Based MOFs having substituents in the organic linkers (UiO-66-X; X = Br, H, or NH_2) as well as the catalytic activities of [–$ArCr(CO)_3$–] complexes for heterogeneous dehydrochlorination of 2-chloro-2-methylbutane. FT–IR, TPD and N_2 adsorption isotherms measurements studies provided evidence that the chemical and physical properties of [–$ArCr(CO)_3$–] complexes were closely similar to that of molecular arenetricarbonyl chromium complexes, suggesting that the [–$ArCr(CO)_3$–] complexes were successfully constructed within UiO-66-type Zr-based MOFs by CVD treatment using $Cr(CO)_6$ as a starting material, i.e., the chromium centers of the complexes were directly coordinated to arene rings belonging to organic linkers of the MOFs, regardless of the type of substituent groups. FT–IR measurements also revealed that the constructed [–$ArCr(CO)_3$–] complexes show a substituent effects similar to molecular arenetricarbonyl chromium complexes, in which peak positions assignable to CO vibrational modes are shifted to lower wavenumber in order of decreased electron withdrawing ability of the substituents. The

catalytic studies revealed that [–ArCr$(CO)_3$–] complexes constructed within UiO-66-NH_2 shows the highest catalytic activity due to the concerted effect between basicity of –NH_2 group and the [–ArCr$(CO)_3$–] complex.

Summary of Chapter 6

Chapter 6 focused on the construction of arenetricarbonyl complexes ([–$C_6H_4M(CO)_3$–]; M = Mo, Cr) within Zr-based MOFs having different pore sizes (UiO-66 and UiO-67) as well as the influence of the pore size of Zr-based MOFs and kinds of metal centers of [–$C_6H_4M(CO)_3$–] complexes on catalytic activities for epoxidation of cyclooctene with tertiary butylhydroperoxide (TBHP). The XRD study revealed the longer organic linker, biphenylene linker, of UiO-67 leads to the expansion of the pore size of UiO-67, as compared to UiO-66. FT–IR and TPD studies provided evidence that the chemical and physical properties of the [–$C_6H_4M(CO)_3$–] complexes were closely similar to that of molecular $C_6H_6Mo(CO)_3$ complexes, suggesting that the [–$C_6H_4M(CO)_3$–] complexes were successfully constructed within UiO-66 and UiO-67 (UiO-66-$M(CO)_3$ and UiO-67-$M(CO)_3$), respectively, through the CVD treatment using $M(CO)_6$ as starting materials. The catalytic studies revealed that the [–$C_6H_4M(CO)_3$–] complexes act as catalytically active sites and the [–$C_6H_4Mo(CO)_3$–] complex exhibit extremely higher catalytic activity than [–$C_6H_4Cr(CO)_3$–] complexes. Furthermore, UiO-67-$Mo(CO)_3$ showed the highest catalytic activity, suggesting that the expansion of pore size of UiO-67-$M(CO)_3$ leads to the improvement of accessibility of substrates to active sites of UiO-67-$M(CO)_3$. The prolonged reaction tests revealed that not only no undesirable side reactions occur on the UiO-67-$Mo(CO)_3$ catalyst but also the UiO-67-$Mo(CO)_3$ catalyst can be reused for the epoxidation of cyclooctene with TBHP at least 2 times.

Acknowledgements

The author, Masakazu Saito, would like to express his sincere gratitude to Professor Masaya Matsuoka of the Department of Applied Chemistry, Graduate School of Engineering, Osaka Prefecture University, for his warm encouragement and invaluable instruction during the course of this study.

Since thanks are also extended to Professor Masahiro Tatsumisago and Professor Hideaki Hisamoto of Osaka Prefecture University for their critical reading of the thesis and for their many useful suggestions for its improvement.

The author also wishes to thank Executive Vice-President Masakazu Anpo, Associate Professor Masato Takeuchi, Assistant Professor Yu Horiuchi of Osaka Prefecture University and Professor Michel Che, Doctor Stanislaw Dzwigaj and Jean-Philippe Nogier of University Pierre et Marie Curie as well as Assistant Professor Takashi Kamegawa of Osaka University for their helpful suggestions and stimulating discussions throughout the present research.

In addition, the author appreciates the help from Professor Masamitsu Shirai, associate Professor Haruyuki Okamura and Kanji Suyama of Osaka Prefecture University as well as Doctor Mayamitsu Miyajima for their encouragement and invaluable instruction.

Deep thanks are also extended to the author's colleagues, Estelle Thouverez, Kozo Ueda, Tetsuji Watanabe, Atsushi Takarada, Hikaru Ikeda, Takuya Hosokawa, Takashi Toyao, Yusuke Yonezawa, Junichi Kawashima, and Kazushi Iyatani for their help and experimental assistance.

Finally, the author likes to express his sincere gratitude to his family, especially his big brother and parents, Hirotaka, Hitoshi and Tomoko Saito, who have always prayed for him well-being and to complete his studies.

Sakai, Osaka, February, 2013

Masakazu Saito

List of Publications

1. Influence of the Ti Content on the Photocatalytic Oxidation of 2-propanol and CO on TiSiBEA Zeolites

   S. Dzwigaj, J.-P. Nogier, M. Che, M. Saito, T. Hosokawa, E. Thouverez, M. Matsuoka, M. Anpo, *Catal. Commun.*, **19**, 17-20 (2012).

2. Synthesis and Application of Tin Triflate–Containing MCM-41 as Heterogeneous Lewis Acid Catalysts for Mukaiyama-Aldol Reaction at Room Temperature

   M. Saito, H. Ikeda, Y. Horiuchi, M. Matsuoka, *Res. Chem. Intermed.*, in press.

3. Construction of an Organoruthenium Complex (–[biphRuCp]PF_6–) within Biphenylene–Bridged Inorganic–Organic Hybrid Mesoporous Materials and Their Catalytic Activity for Selective Hydrosilylation of 1-Hexyne

   M. Saito, T. Watanabe, Y. Horiuchi, T. Kamegawa, M. Matsuoka, *Res. Chem. Intermed.*, in press.

4. Enhanced Catalytic Activity of Arenetricarbonyl Chromium Complexes Constructed within Zr-Based MOFs by Introducing Substituents into Organic Linkers of the MOFs

   M. Saito, K. Ueda, Y. Horiuchi, T. Kamegawa, M. Matsuoka, *Chem. Commun.*, submitted.

5. Effect of Pore Size on Catalytic Activities of Arenetricarbonyl Complexes ([–$C_6H_4M(CO)_3$–]; M = Mo, Cr) Constructed within Zr-Based MOFs

   M. Saito, K. Ueda, Y. Horiuchi, T. Kamegawa, M. Matsuoka, *Phys. Chem. Chem. Phys.*, submitted.